Appendix A

AsCNAR

Quadratic Regression

The $\log_2$ signal-ratio, $\log_2 R^{refI}_{AB,i}$ is regressed by the quadratic terms (the length $[L_i]$ and the GC content $[M_i]$ of the PCR fragment of the ith SNP) as

$$\log_2 R^{refI}_{AB,i} = \alpha L_i^2 + \beta L_i + \chi M_i^2 + \delta M_i + \gamma + \varepsilon_i \ ,$$

where ε_i is the error term and the coefficients of regressions α, β, χ, δ, and γ are dependent on the reference used and are determined to minimize the residual sum of squares (i.e., $\Sigma_i \varepsilon_i^2$). Note that the sum is taken for those SNPs that have concordant SNP calls between the tumor and the reference samples.

We suppose that both allele A DNA and allele B DNA follow the same PCR kinetics, and allele-specific ratios $R^{refI}_{A,i}$ and $R^{refI}_{B,i}$, respectively, can be regressed by the same parameters, as

$$\log_2 \hat{R}^{refI}_{A,i} = \log_2 R^{refI}_{A,i} - (\alpha L_i^2 + \beta L_i) - (\chi M_i^2 + \delta M_i) - \gamma$$

and

$$\log_2 \hat{R}^{refI}_{B,i} = \log_2 R^{refI}_{B,i} - (\alpha L_i^2 + \beta L_i) - (\chi M_i^2 + \delta M_i) - \gamma \ ,$$

and the corrected total CN ratio is

$$\hat{R}^{refI}_{AB,i} = \begin{cases} \hat{R}^{refI}_{A,i} & \text{for } O_i^{tum} = O_i^{refI} = AA \\ \hat{R}^{refI}_{B,i} & \text{for } O_i^{tum} = O_i^{refI} = BB \\ \frac{1}{2}(\hat{R}^{refI}_{A,i} + \hat{R}^{refI}_{B,i}) & \text{for } O_i^{tum} = O_i^{refI} = AB \end{cases} .$$

Averaging over the References of Concordance SNPs

Concordant reference sets C_i^K and $C_i^{K,hetero}$ for each SNP S_i for a given set of references, K, are defined as follows:

$$C_i^K = \{refI \mid O_i^{tum} = O_i^{refI}, refI \in K\}$$

$$C_i^{K,hetero} = \{refI \mid O_i^{tum} = O_i^{refI} = AB, refI \in K\} \ ,$$

and the averaged CN ratio, $\bar{R}^K_{AB,i}$, is provided by

$$\bar{R}^K_{AB,i} = \frac{1}{\#C_i^K} \sum_{refI \in C_i^K} \hat{R}^{refI}_{AB,i} \ , \ C_i^K \neq \phi$$

where "#" denotes the number of the elements of the set. Similarly, AsCN ratios are obtained by

$$\bar{R}^K_{A,i} = \frac{1}{\#C_i^{K,hetero}} \sum_{refI \in C_i^{K,hetero}} \hat{R}^{refI}_{A,i}$$

$$(C_i^{K,hetero} \neq \phi) \ .$$

$$\bar{R}^K_{B,i} = \frac{1}{\#C_i^{K,hetero}} \sum_{refI \in C_i^{K,hetero}} \hat{R}^{refI}_{B,i}$$

Exceptional Handling with Regions of Homozygous Deletion, High Amplification, and LOH

To prevent SNPs within the regions that show homozygous deletion or high-grade amplification from being analyzed as "homozygous SNPs," a homozygous SNP S_i in the tumor sample is redefined as a heterozygous SNP with $\hat{O}_i^{tum} = AB$, if $\max(\log_2 \bar{R}^K_{A,i}, \log_2 \bar{R}^K_{B,i}) \leq 0.1$ or $\min(\log_2 \bar{R}^K_{A,i}, \log_2 \bar{R}^K_{B,i}) \geq -0.1$, where $\bar{R}^K_{A,i}$ and $\bar{R}^K_{B,i}$ are calculated supposing SNP S_i is heterozygous. These cutoff values (0.1 and −0.1) are determined by receiver operating characteristic (ROC) curve for detection of gain of the larger allele and loss of the smaller allele in a sample containing 20% tumor cells (data not shown). In addition, SNPs within inferred LOH regions are also analyzed as "heterozygous" SNPs.

Reference Selection

The optimized set of references is selected that minimizes the SD of total CN at the diploid region D,

$$SD_K(D) = \sqrt{\frac{\sum_{i \in D, C_i^K \neq \phi} (\log_2 \bar{R}^K_{AB,i})^2}{\#\{i \mid i \in D, C_i^K \neq \phi\} - 1}} \ .$$

To do this, instead of testing all possible 2^N combinations of N references, we calculate $SD_K(D)$ for individual references $K = \{ref1\}, \{ref2\}, \{ref3\}, \ldots, \{refN\}$, to order the references such that $SD_1(D) \leq \ldots \leq SD_s(D) \leq SD_{s+1}(D) \leq \ldots \leq SD_N(D)$, where 1, 2, 3,...,$s$, $s+1$,..., N denotes the ordered references. The optimal set $K(N_0) = \{1,2,3,\ldots,N_0\}$ is determined by choosing N_0 that satisfies $SD_{K(1)}(D) \geq \ldots \geq SD_{K(N_0)}(D) < SD_{K(N_0+1)}(D)$.

Note that, in principle, a diploid region cannot be unequivocally determined without doing single-cell–based analysis—for example, FISH or cytogenetics. Otherwise, a diploid region is empirically determined by setting the CN-minimal regions with no AI as diploid, which provides correct estimation of the ploidy in most cases (data not shown).

The figure is available in its entirety in the online edition of *The American Journal of Human Genetics*.

Figure C1. Inference of LOH on the basis of heterozygous SNP calls. The legend is available in its entirety in the online edition of *The American Journal of Human Genetics*.

Appendix C
Inference of LOH Based on Heterozygous SNP Calls

For a given contiguous region $\Omega_{i,j}$ between the ith and jth SNPs ($i \leq j$) and for the complete set of observed SNP calls therein, $O(\Omega_{i,j})$, consider the log likelihood ratio

$$Z(\Omega_{i,j}) \equiv \ln \frac{P(O(\Omega_{i,j}) | \Omega_{i,j} \in \text{LOH})}{P(O(\Omega_{i,j}) | \Omega_{i,j} \notin \text{LOH})},$$

where the ratio is taken between the conditional probabilities that the current observation, $O(\Omega_{i,j})$, is obtained under the assumption that $O(\Omega_{i,j})$ belongs to LOH or not. We assume a constant miscall rate ($q = 0.001$) for all SNP and use the conditional probability that the kth SNP is heterozygous (h_k), depending on the observed $k-1$th SNP call, for partially taking the effect of linkage disequilibrium into account:

$$Z(\Omega_{i,j}) = \ln \frac{\prod_{i \leq k \leq j} \{(1-q)O_k + q(1-O_k)\}}{\prod_{i \leq k \leq j} [\{(1-h_k)(1-q) + h_k q\}O_k + \{(1-h_k)q + h_k(1-q)\}(1-O_k)]}$$

where h_k is calculated using the data from the 96 normal Japanese individuals, whereas O_k takes either 1 or 0, depending on the kth SNP call, with 1 for a homozygous call and 0 for a heterozygous call. For each chromosome, a set of regions, $\Omega_{I_n,J_n}(J_{n-1} < I_n \leq J_n, J_0 = 0)$ ($n = 1,2,3,\ldots$), can be uniquely determined as follows.

Beginning with the SNP at the short arm end (S_0), find the SNP S_{I_n} that satisfies $Z(\Omega_{I_n,I_n}) > 0$ and $Z(\Omega_{i,i}) \leq 0$ for $J_{n-1} < \forall i < I_n$ (fig. C1). Identify the SNP S_J, such that $Z(\Omega_{I_n,j}) > 0$ for $I_n \leq \forall j \leq J^+$ and $Z(\Omega_{I_n,J^+1}) \leq 0$, or that S_J is the end of the chromosome (fig. C1). Then, put J_n as $\arg\max_j Z(\Omega_{I_n,j})(I_n \leq j \leq J^+)$ (fig. C1). This procedure is iteratively performed, beginning the next iteration with the SNP $S_{I_{n+1}}$, until it reaches to the end of the long arm, generating a set of nonoverlapping regions, $\Omega_{I_1,J_1}, \Omega_{I_2,J_2}, \Omega_{I_3,J_3}, \ldots \Omega_{I_n,J_n}, \ldots$. LOH inference is now enabled by testing each $Z(\Omega_{I_n,J_n})$ against a threshold (25), which is arbitrarily determined from the ROC curve for LOH determination on a DNA sample from a lung cancer cell line, NCI-H2171 (fig. C1). This algorithm is implemented in our CNAG program, which is available at our Web site.

Appendix E
Algorithm for Detection of AI With or Without LOH

The regions with AI are inferred from the AsCN data by use of an HMM, where the real state of AI (a hidden state) is inferred from the observed states of difference in AsCNs of the two parental alleles, which are expressed as dichotomous values ("preset" or "absent") according to a threshold (μ). The emission probabilities at the ith SNP locus (Si) are

$$P(|\log_2 \bar{R}^K_{A,i} - \log_2 \bar{R}^K_{B,i}| \leq \mu | Si \in \text{AI}) = \beta$$

$$P(|\log_2 \bar{R}^K_{A,i} - \log_2 \bar{R}^K_{B,i}| > \mu | Si \in \text{AI}) = 1 - \beta$$

and

$$P(|\log_2 \bar{R}^K_{A,i} - \log_2 \bar{R}^K_{B,i}| > \mu | Si \in \overline{\text{AI}}) = \alpha$$

$$P(|\log_2 \bar{R}^K_{A,i} - \log_2 \bar{R}^K_{B,i}| \leq \mu | Si \in \overline{\text{AI}}) = 1 - \alpha$$

(see also the "Material and Methods" section and appendix A for calculation of $\bar{R}^K_{A,i}$ and $\bar{R}^K_{B,i}$).

The parameters (μ, α, and β) are determined by the results of 10%, 20%, and 30% tumor samples. Sensitivity and specificity are calculated with varying threshold (μ), where sensitivity is defined as the ratio of detected SNPs of UPD region detected in the 100% tumor sample, specificity is defined as the ratio of nondetected SNPs in normal samples, and α and β parameters are determined from mixed tumor-sample data for each threshold value. Sensitivity and specificity are relatively stable and are within the acceptable range when the threshold is between 0.05 and 0.15 in 20% and 30% tumor samples (fig. E1). We used 0.12, 0.17, and 0.06 for μ, α, and β, respectively, on the basis of 20% tumor-sample data.

Considering that UPD is caused by a process similar to recombination, the Kosambi's map function $(1/2)\tanh(2\theta)$ is used for transition probability, where θ is the distance between two SNPs, expressed in cM units; for simplicity, 1 cM should be 1 Mbp. Thus, the most likely underlying, hidden, real states of AI are calculated for each SNP according to Vitervi's method, by which AI-positive regions are defined by contiguous SNPs with "present" AI calls flanked by either chromosomal end or an "absent" AI call. Next, to determine the LOH status for each AI-positive region (Γ), AsCN states at each SNP locus within Γ are

The figure is available in its entirety in the online edition of *The American Journal of Human Genetics*.

Figure E1. Sensitivity and specificity for determination of AI, LOH, and UPD. The legend is available in its entirety in the online edition of *The American Journal of Human Genetics*.

inferred as "reduced (R)" and "not reduced ($\bar{R}$)" for the smaller AsCNs, and "increased (I)" and "not increased ($\bar{I}$)" for the larger AsCNs, using similar HMMs from the "observed CN states" of the smaller and the larger AsCNs, which are expressed as dichotomous values according to thresholds μ_S and μ_L, respectively. The emission probabilities of these models are

$$P[\min(\log_2 \bar{R}^K_{A,i}, \log_2 \bar{R}^K_{B,i}) < \mu_S \mid Si \in R] = 1 - \beta_S$$

$$P[\min(\log_2 \bar{R}^K_{A,i}, \log_2 \bar{R}^K_{B,i}) \geq \mu_S \mid Si \in R] = \beta_S$$

$$P[\min(\log_2 \bar{R}^K_{A,i}, \log_2 \bar{R}^K_{B,i}) < \mu_S \mid Si \in \bar{R}] = \alpha_S$$

$$P[\min(\log_2 \bar{R}^K_{A,i}, \log_2 \bar{R}^K_{B,i}) \geq \mu_S \mid Si \in \bar{R}] = 1 - \alpha_S$$

and

$$P[\max(\log_2 \bar{R}^K_{A,i}, \log_2 \bar{R}^K_{B,i}) > \mu_L \mid Si \in I] = 1 - \beta_L$$

$$P[\max(\log_2 \bar{R}^K_{A,i}, \log_2 \bar{R}^K_{B,i}) \leq \mu_L \mid Si \in I] = \beta_L$$

$$P[\max(\log_2 \bar{R}^K_{A,i}, \log_2 \bar{R}^K_{B,i}) > \mu_L \mid Si \in \bar{I}] = \alpha_L$$

$$P[\max(\log_2 \bar{R}^K_{A,i}, \log_2 \bar{R}^K_{B,i}) \leq \mu_L \mid Si \in \bar{I}] = 1 - \alpha_L .$$

These parameters (μ_S, α_S, β_S, μ_L, α_L, and β_L) are determined by evaluating sensitivities and specificities of the results for 10%, 20%, and 30% tumor samples, where sensitivities and specificities are calculated the same way as was AI. Sensitivity and specificity are relatively stable for μ_S between -0.03 and -0.13 and are relatively stable for μ_L between 0.04 and 0.09 in 20% and 30% tumor samples (fig. E1). We employed $\mu_S = -0.1$, $\alpha_S = 0.3$, $\beta_S = 0.26$, $\mu_L = 0.08$, $\alpha_L = 0.27$, and $\beta_L = 0.31$ on the basis of the data for 20% tumor content.

Web Resources

The URLs for data presented herein are as follows:

ATCC, http://www.atcc.org/common/cultures/NavByApp.cfm
BACPAC Resources Center, http://bacpac.chori.org/
CNAG, http://www.genome.umin.jp/
dChip, http://www.dchip.org/
Online Mendelian Inheritance in Man (OMIM), http://www.ncbi.nlm.nih.gov/Omim/ (for *JAK2*, AML, PV, ET, and IMF)
PLASQ, http://genome.dfci.harvard.edu/~tlaframb/PLASQ/

References

1. Mei R, Galipeau PC, Prass C, Berno A, Ghandour G, Patil N, Wolff RK, Chee MS, Reid BJ, Lockhart DJ (2000) Genome-wide detection of allelic imbalance using human SNPs and high-density DNA arrays. Genome Res 10:1126–1137
2. Horvath A, Boikos S, Giatzakis C, Robinson-White A, Groussin L, Griffin KJ, Stein E, Levine E, Delimpasi G, Hsiao HP, et al (2006) A genome-wide scan identifies mutations in the gene encoding phosphodiesterase 11A4 (*PDE11A*) in individuals with adrenocortical hyperplasia. Nat Genet 38:794–800
3. Lindblad-Toh K, Tanenbaum DM, Daly MJ, Winchester E, Lui WO, Villapakkam A, Stanton SE, Larsson C, Hudson TJ, Johnson BE, et al (2000) Loss-of-heterozygosity analysis of small-cell lung carcinomas using single-nucleotide polymorphism arrays. Nat Biotechnol 18:1001–1005
4. Knudson AG (2001) Two genetic hits (more or less) to cancer. Nat Rev Cancer 1:157–162
5. Baxter EJ, Scott LM, Campbell PJ, East C, Fourouclas N, Swanton S, Vassiliou GS, Bench AJ, Boyd EM, Curtin N, et al (2005) Acquired mutation of the tyrosine kinase JAK2 in human myeloproliferative disorders. Lancet 365:1054–1061
6. James C, Ugo V, Le Couedic JP, Staerk J, Delhommeau F, Lacout C, Garcon L, Raslova H, Berger R, Bennaceur-Griscelli A, et al (2005) A unique clonal JAK2 mutation leading to constitutive signalling causes polycythaemia vera. Nature 434:1144–1148
7. Kralovics R, Passamonti F, Buser AS, Teo SS, Tiedt R, Passweg JR, Tichelli A, Cazzola M, Skoda RC (2005) A gain-of-function mutation of JAK2 in myeloproliferative disorders. N Engl J Med 352:1779–1790
8. Levine RL, Wadleigh M, Cools J, Ebert BL, Wernig G, Huntly BJ, Boggon TJ, Wlodarska I, Clark JJ, Moore S, et al (2005) Activating mutation in the tyrosine kinase JAK2 in polycythemia vera, essential thrombocythemia, and myeloid metaplasia with myelofibrosis. Cancer Cell 7:387–397
9. Kennedy GC, Matsuzaki H, Dong S, Liu WM, Huang J, Liu G, Su X, Cao M, Chen W, Zhang J, et al (2003) Large-scale genotyping of complex DNA. Nat Biotechnol 21:1233–1237
10. Zhao X, Li C, Paez JG, Chin K, Janne PA, Chen TH, Girard L, Minna J, Christiani D, Leo C, et al (2004) An integrated view of copy number and allelic alterations in the cancer genome using single nucleotide polymorphism arrays. Cancer Res 64:3060–3071
11. Huang J, Wei W, Zhang J, Liu G, Bignell GR, Stratton MR, Futreal PA, Wooster R, Jones KW, Shapero MH (2004) Whole genome DNA copy number changes identified by high density oligonucleotide arrays. Hum Genomics 1:287–299
12. Bignell GR, Huang J, Greshock J, Watt S, Butler A, West S, Grigorova M, Jones KW, Wei W, Stratton MR, et al (2004) High-resolution analysis of DNA copy number using oligonucleotide microarrays. Genome Res 14:287–295
13. Wang ZC, Buraimoh A, Iglehart JD,Richardson AL (2006) Genome-wide analysis for loss of heterozygosity in primary and recurrent phyllodes tumor and fibroadenoma of breast using single nucleotide polymorphism arrays. Breast Cancer Res Treat 97:301–309
14. Zhou X, Mok SC, Chen Z, Li Y, Wong DT (2004) Concurrent analysis of loss of heterozygosity (LOH) and copy number abnormality (CNA) for oral premalignancy progression using the Affymetrix 10K SNP mapping array. Hum Genet 115:327–330
15. Matsuzaki H, Dong S, Loi H, Di X, Liu G, Hubbell E, Law J, Berntsen T, Chadha M, Hui H, et al (2004) Genotyping over 100,000 SNPs on a pair of oligonucleotide arrays. Nat Methods 1:109–111
16. Nannya Y, Sanada M, Nakazaki K, Hosoya N, Wang L, Hangaishi A, Kurokawa M, Chiba S, Bailey DK, Kennedy GC, et al (2005) A robust algorithm for copy number detection using high-density oligonucleotide single nucleotide polymorphism genotyping arrays. Cancer Res 65:6071–6079
17. Beroukhim R, Lin M, Park Y, Hao K, Zhao X, Garraway LA, Fox EA, Hochberg EP, Mellinghoff IK, Hofer MD, et al (2006) Inferring loss-of-heterozygosity from unpaired tumors using

high-density oligonucleotide SNP arrays. PLoS Comput Biol 2:e41
18. Laframboise T, Harrington D, Weir BA (2007) PLASQ: a generalized linear model-based procedure to determine allelic dosage in cancer cells from SNP array data. Biostatistics 8: 323–336
19. Kralovics R, Teo SS, Li S, Theocharides A, Buser AS, Tichelli A, Skoda RC (2006) Acquisition of the V617F mutation of JAK2 is a late genetic event in a subset of patients with myeloproliferative disorders. Blood 108:1377–1380
20. Wang L, Ogawa S, Hangaishi A, Qiao Y, Hosoya N, Nanya Y, Ohyashiki K, Mizoguchi H, Hirai H (2003) Molecular characterization of the recurrent unbalanced translocation der(1;7)(q10;p10). Blood 102:2597–2604
21. Huang J, Wei W, Chen J, Zhang J, Liu G, Di X, Mei R, Ishikawa S, Aburatani H, Jones KW, et al (2006) CARAT: a novel method for allelic detection of DNA copy number changes using high density oligonucleotide arrays. BMC Bioinformatics 7:83
22. Dugad R, Desai U (1996) A tutorial on hidden Markov models. Technical report SPANN-96.1. Signal Processing and Artificial Neural Networks Laboratory, Bombay, India
23. Raghavan M, Lillington DM, Skoulakis S, Debernardi S, Chaplin T, Foot NJ, Lister TA, Young BD (2005) Genome-wide single nucleotide polymorphism analysis reveals frequent partial uniparental disomy due to somatic recombination in acute myeloid leukemias. Cancer Res 65:375–378
24. Fitzgibbon J, Smith LL, Raghavan M, Smith ML, Debernardi S, Skoulakis S, Lillington D, Lister TA, Young BD (2005) Association between acquired uniparental disomy and homozygous gene mutation in acute myeloid leukemias. Cancer Res 65:9152–9154
25. Najfeld V, Montella L, Scalise A, Fruchtman S (2002) Exploring polycythaemia vera with fluorescence in situ hybridization: additional cryptic 9p is the most frequent abnormality detected. Br J Haematol 119:558–566
26. Peiffer DA, Le JM, Steemers FJ, Chang W, Jenniges T, Garcia F, Haden K, Li J, Shaw CA, Belmont J, et al (2006) High-resolution genomic profiling of chromosomal aberrations using Infinium whole-genome genotyping. Genome Res 16: 1136–1148
27. Scott LM, Scott MA, Campbell PJ, Green AR (2006) Progenitors homozygous for the V617F mutation occur in most patients with polycythemia vera, but not essential thrombocythemia. Blood 108:2435–2437

THE JOURNAL OF BIOLOGICAL CHEMISTRY VOL. 282, NO. 18, pp. 13875–13883, May 4, 2007

The Nuclear Import of the Human T Lymphotropic Virus Type I (HTLV-1) Tax Protein Is Carrier- and Energy-independent*

Received for publication, December 19, 2006, and in revised form, March 6, 2007 Published, JBC Papers in Press, March 6, 2007, DOI 10.1074/jbc.M611629200

Takahiro Tsuji[‡], Noreen Sheehy[‡], Virginie W. Gautier[‡], Hitoshi Hayakawa[‡], Hirofumi Sawa[§], and William W. Hall[‡1]

From the [‡]Centre for Research in Infectious Disease, School of Medicine & Medical Science, University College Dublin, Belfield, Dublin 4, Ireland and the [§]Department of Molecular Pathobiology and 21st Century COE Program for Zoonosis Control, Hokkaido University Research Center for Zoonosis Control, N18, W9, Kita-ku, Sapporo, 060-0818, Japan

HTLV-1 is the etiologic agent of the adult T cell leukemia-lymphoma (ATLL). The viral regulatory protein Tax plays a central role in leukemogenesis as a transcriptional transactivator of both viral and cellular gene expression, and this requires Tax activity in both the cytoplasm and the nucleus. In the present study, we have investigated the mechanisms involved in the nuclear localization of Tax. Employing a GFP fusion expression system and a range of Tax mutants, we could confirm that the N-terminal 60 amino acids, and specifically residues within the zinc finger motif in this region, are important for nuclear localization. Using an *in vitro* nuclear import assay, it could be demonstrated that the transportation of Tax to the nucleus required neither energy nor carrier proteins. Specific and direct binding between Tax and p62, a nucleoporin with which the importin beta family of proteins have been known to interact was also observed. The nuclear import activity of wild type Tax and its mutants and their binding affinity for p62 were also clearly correlated, suggesting that the entry of Tax into the nucleus involves a direct interaction with nucleoporins within the nuclear pore complex (NPC). The nuclear export of Tax was also shown to be carrier independent. It could be also demonstrated that Tax it self may have a carrier function and that the NF-κB subunit p65 could be imported into the nucleus by Tax. These studies suggest that Tax could alter the nucleocytoplasmic distribution of cellular proteins, and this could contribute to the deregulation of cellular processes observed in HTLV-1 infection.

Human T cell lymphotropic virus type-I (HTLV-1)[2] is the etiologic agent of the malignant disorder adult T cell leukemia-lymphoma (ATLL) (1, 2). Whereas the pathogenesis of ATLL is unclear, the HTLV-1 regulatory protein Tax is thought to play a central role in leukemogenesis. Tax has been shown to immortalize human T cells (3) and transform fibroblast cells (4) *in vitro*, and transgenic animals expressing Tax have developed a range of malignancies (5–8). The mechanisms of the transformation are not fully understood, but have been shown to be related to the ability of Tax to dysregulate the transcription of genes involved in cellular proliferation, cell-cycle control, and apoptosis (9–11). Tax is a potent transcriptional transactivator not only of viral but also of cellular gene expression. The protein physically interacts with a number of cellular transcription factors, which including components of the NF-κB-Rel signaling complex, and persistent and constitutive activation of NF-κB is central to the development and maintenance of the malignant phenotype in ATLL (10–12).

Activation of NF-κB involves Tax activity in both the cytoplasm and nucleus. In the cytoplasm, Tax activates the kinase activity of IKK complex by directly interacting with IKKγ/NEMO subunit. IκBα, which sequesters NF-κB in the cytoplasm, is phosphorylated by the Tax-IKK complex and subsequently degraded allowing the nuclear translocation of NF-κB (13). In the nucleus, Tax has also been shown to co-localize with NF-κB as well as basic transcriptional factors such as p300/CBP in nuclear speckle structures, the so-called Tax speckle structure (TSS), where active transcription of a range of cellular genes occurs (14, 15).

Consistent with both its cytoplasmic and nuclear activities, Tax has been shown to be distributed in both compartments in HTLV-1-infected and Tax-transfected cells. In initial studies, Tax was reported to be found predominantly in the nucleus and specifically accumulated in the nuclear speckled structures (16, 17). However, depending on the cell type, significant amounts of Tax have also been found in the cytoplasm (18–20). Specifically, cytoplasmic Tax was shown to co-localize in the endoplasmic reticulum, Golgi apparatus, and mitotic organizing center (MTOC), and appeared to affect both protein secretion and microtubule organization (21, 22). Recent studies employing a heterokaryon fusion system have also clearly demonstrated that Tax can effectively shuttle between the cytoplasm and the nucleus (18).

Nuclear transport of proteins occur through the nuclear pore complex (NPC), and in most cases involves an interaction between transport carriers and a nuclear localization signal (NLS) on the cargo protein (23, 24). Most transport carriers belongs to the importin (karyopherin) family and mediate transport either as monomers and heterodimers. Importin α/β heterodimers import cargo proteins containing a "classical" NLS which is generally rich in lysine residues (23). Importin β monomer imports a range of cargo proteins including the parathyroid hormone-related protein (25), the sterol regulatory

* The costs of publication of this article were defrayed in part by the payment of page charges. This article must therefore be hereby marked "*advertisement*" in accordance with 18 U.S.C. Section 1734 solely to indicate this fact.

[1] To whom correspondence should be addressed. Tel.: 353-1-716-1229; Fax: 353-1-716-1239; E-mail: william.hall@ucd.ie.

[2] The abbreviations used are: HTLV-1, human T cell lymphotropic virus type-I; GST, glutathione *S*-transferase; WGA, wheat germ agglutinin; GFP, green fluorescent protein; MAPK, mitogen-activated protein kinase; TSS, Tax speckle structure; NPC, nuclear pore complex; ATLL, adult T cell leukemia-lymphoma; RRL, rabbit reticulocyte lysate; DAPI, 4′,6-diamidino-2-phenylindole; WT, wild type.

element-binding protein 2 (SREBP-2) (26), the zinc finger protein Snail (27), as well as the viral proteins HIV-1 Rev (28, 29) and HTLV-1 Rex (30). Transportin monomer, which also belongs to the importin β family, imports cargo proteins such as hnRNP A1 protein (31), several kinds of histones (32) and ribosomal proteins (33). The import process requires metabolic energy and is propelled by a concentration gradient across the nuclear envelope of the GTP-bound form of small GTPase Ran, which is found at high concentrations in the nucleus (23). In contrast, the transport of a number of other proteins is carrier independent; these include β-catenin (34), MAPK (35, 36), SMAD (37), STAT (38), HIV-1 Vpr (39), RCC1 (40), and PU.1 (41) all of which have been shown to translocate through the nuclear pore complex (NPC) in the apparent absence of a carrier protein.

While the N-terminal ~60 amino acids of Tax has been shown to be important for the nuclear localization of Tax (42–44), there is no similarity between the amino acid sequences in this region and those of the other NLSs so far reported, and the mechanism by which Tax is transported into the nucleus has remained unclear. In the present study, we have analyzed the nuclear import of Tax using an *in vitro* nuclear import assay system which allows manipulation of the soluble components and selective reconstitution of the nuclear import process *in vitro* using exogeneous substrates. Our results demonstrate that Tax is imported into the nucleus through the NPC by directly interacting with components of the NPC and this is both energy independent and does not require a carrier protein. Notably our studies also show that Tax itself may function as a carrier protein permitting the nuclear translocation of a number of cellular proteins and this may in turn contribute to the dysregulation of cell function which occurs in HTLV-1 infection.

EXPERIMENTAL PROCEDURES

Cell Culture and Transfection—HeLa and COS7 cells were maintained in Dulbecco's minimal essential medium supplemented with 10% fetal bovine serum and penicillin/streptomycin. HeLa cells were plated on 18-well printed slides (Roboz Surgical Instrument Co., Inc., Gaithersburg, MD) for the *in vitro* nuclear import assays 24 h before the experiments. COS7 cells were plated on two-well chamber slides (Nalge Nunc International, Naperville, IL) 24 h before transfection. Cells were transfected with 1 μg of plasmids using FuGENE6 (Roche Diagnostics, Mannheim, Germany).

DNA Construction and Plasmids—To create mammalian expression vectors for GFP-Tax/-Tax340/-Tax220/-Tax116/-Tax60/-Tax55/-Tax50, cDNA sequences encoding full-length Tax and the series of C-terminal deletion mutants were amplified by PCR and cloned into the HindIII/PstI sites of the pEGFP-C1 vector (Clontech).

The bacterial expression vectors for the SV40 T antigen NLS, GST-SV40TNLS-GFP (pGEX-SV40TNLS-GFP), GST-HA-importin β (pGEX-HA-importin β), GST-importin β (pGEX-importin β), and His_6-RanQ69L (pQE80-RanQ69L) were gifts from Dr. S. Kose and Dr. N. Imamoto (RIKEN, Saitama, Japan). To create the bacterial expression vectors for GST-Tax-GFP and GST-Tax340-GFP, the SV40-T-antigen NLS coding sequences of pGEX-SV40TNLS-GFP were swapped for the Tax and Tax1–340 coding sequences by utilizing BamHI/SmaI sites of the vector. To create bacterial expression vectors for GST-Tax340-CFP and GST-YFP-Rev, Tax1–340, and CFP encoding sequences from pECFP-C1 (Clontech) were cloned into the BamHI and SmaI sites of pGEX-2T vector (Amersham Biosciences), and YFP encoding sequences from pEYFP-C1 (Clontech) and HIV-1 Rev encoding sequences were cloned into the SmaI and EcoRI sites of pGEX-2T vector. To construct bacterial expression vector for GST-Tax, Tax encoding sequences were cloned into the BamHI site of pGEX-2T vector. The bacterial expression vectors for GST-p62FL [1–522], GST-p62N [1–265] and GST-p62C [178–522] were generated by cloning relevant sequences (41) from pcDNA3.1/His-p62 vector (a gift from Dr. N. Yaseen, Northwestern University, Chicago, IL) into pGEX-2T vector. To construct the bacterial expression vector expressing His_6-p65-YFP, p65 encoding sequencing amplified from pcDNA-p65 vector (a gift from Dr. D. Walls, Dublin City University, Dublin, Ireland) and YFP encoding sequences amplified from pEYFP-C1 (Clontech) vector were cloned into the BamHI and PstI sites of pQE80 (Qiagen) vector. QuikChange™ site-directed mutagenesis kit (Stratagene) was used for the creation of single amino acid mutations in Tax-encoding sequences.

Expression and Purification of Recombinant Proteins—All GST and His fusion proteins were purified from *Escherichia coli* strain BL21(DE) induced with 0.5 mM isopropyl-β-D-thiogalactopyranoside for 14 h at 18 °C. Purifications were performed on glutathione-Sepharose 4B beads (Amersham Biosciences) for the GST fusions and on Ni-NTA agarose beads (Qiagen) for the His fusions, according to the manufacturer's protocols. Tax-/TaxC23A-/TaxC29A-/TaxC36A-/TaxH41A-GFP, Tax340-GFP/-CFP, and HA-importin β were cleaved from GST by using thrombin. To obtain RanQ69L-GTP, 2 mM EDTA, 2 mM GTP, and 5 mM $MgCl_2$ were added to His_6-RanQ69L, which had been eluted from resin and incubated for 30 min on ice. All resultant proteins were dialyzed against transport buffer (TB; 20 mM HEPES, pH7.3, 110 mM potassium acetate, 2 mM magnesium acetate, 5 mM sodium acetate, 0.5 mM EGTA, 2 mM dithiothreitol, 1 μg/ml aprotinin, leupeptin, and pepstatin A), and concentrated by ultrafiltration on Microcon (Amicon), and stored at −80 °C after snap freezing.

In Vitro Nuclear Transport Assay—*In vitro* nuclear import assays were performed essentially as described previously (34, 45). HeLa cells plated on glass slides were washed twice with ice-cold TB and permeabilized with digitonin (40 μg/ml, Sigma) in TB for 5 min on ice. Cells were then washed twice with ice-cold TB and soaked in TB for 10 min on ice. The standard reaction mixtures contained import substrates (~1 μM), an ATP regeneration system (1 mM ATP, 5 mM phosphocreatine, 20 units of creatine kinase) as a source of energy, and rabbit reticulocyte lysate (RRL, Promega) as a source of soluble import factors. The import reaction was performed for 20 min at 30 °C or on ice. For the export reactions, the cells initially subjected to the import reaction were immediately washed twice with TB and then were incubated with testing solutions for 20 min at 30 °C to examine export. The composition of each of the reaction mixtures are described in each figure legend. After the

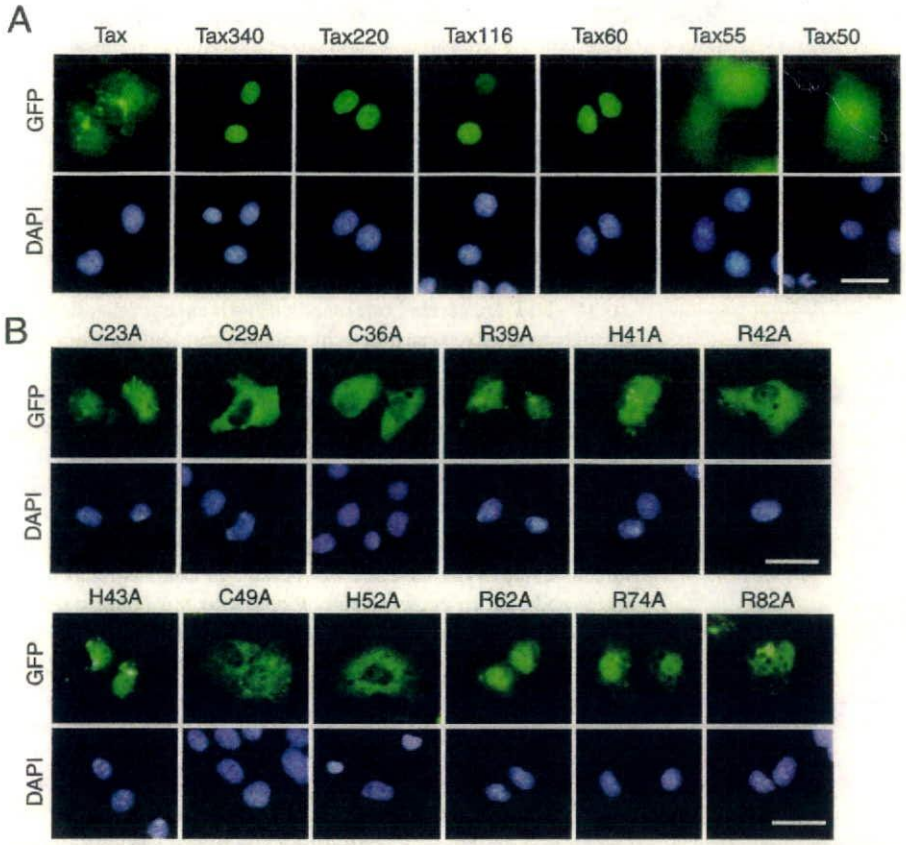

FIGURE 1. **The N-terminal 60 amino acids of Tax are necessary for the nuclear localization of Tax.** COS7 cells were transiently transfected with GFP-Tax and GFP-Tax-C-terminal deletion mutants (*A*) or GFP-Tax with single amino acid mutants (*B*). Twenty-four hours later, cells were fixed and counterstained with DAPI. Representative images of transfected cells were demonstrated. *Scale bars*, 20 μm.

transport reactions, the cells were washed twice with TB followed by fixation with 4% paraformaldehyde for 8 min at room temperature. The cells were washed twice with TB and mounted with 50% glycerol in TB, and examined by fluorescence microscopy. Fluorescent intensities in nuclei and in randomly chosen areas outside the nuclei were quantified by using ImageJ software (NIH).

Protein Binding Assay—Recombinant GST or GST fusion proteins were incubated with HA-importin β or GFP fusion proteins in a total volume of 100 μl in TB with 3% bovine serum albumin. After incubation for 20 min at room temperature, 10 μl of glutathione-Sepharose 4B beads were added to the reaction mixtures and incubated for 30 min at room temperature. The bead complexes were then washed four times with 500 μl each of TB. Bound proteins were eluted from the beads with 25 μl of 10 mM reduced glutathione and analyzed by SDS-PAGE and immunoblotting. In immunoblotting, rabbit anti-GFP antibody (ab290, Abcam, UK) and mouse anti-HA antibody (HA-7, Sigma) were used, and the antibody detection was performed using the Superfemto chemiluminescent kit (Pierce).

RESULTS

The N Terminal 60 Amino Acids Are Important for the Nuclear Accumulation of Tax—Tax has been known to localize primarily in the nucleus in HTLV-1-infected or Tax-transfected cells (15,16,22,42–44,46). The 60 amino acids of the N terminus of Tax have been shown to be necessary for its nuclear localization, as fusion of this region permits nuclear localization of heterogeneous proteins, and deletion of the region results in the complete loss of Tax nuclear localization (42–44).

To confirm and extend these findings, we employed a GFP fusion protein system as this has been widely utilized in subcellular localization analyses of a number of proteins including Tax (19, 20, 47). DNA fragments encoding a full-length Tax or a series of C-terminal deletion mutants of Tax were inserted into the C terminus of a GFP expression vector, and their subcellular localizations were examined (Fig. 1*A*). As previously reported, GFP with full-length Tax localized both in the nucleus and in the cytoplasm with a speckled pattern (Fig. 1*A*) (20, 21). GFP with C-terminal deletions (Tax340, Tax220, Tax116, and Tax60 and as well as Tax280; Fig. 1*A*, and not shown) accumulated almost exclusively in the nucleus. Of note, Tax340, a mutant with the deletion of only the C-terminal 13 amino acids, completely lost its cytoplasmic localization pattern. Tax C-terminal deletion mutants shorter than Tax60 resulted in the leakage of the fusion protein into the cytoplasm (Tax55 and Tax50 as well as Tax45; Fig. 1*A*, and not shown). Therefore, as has been previously shown (42–44), it could be confirmed that the N-terminal 60 amino acids of Tax were the minimal region permitting the localization of the GFP fusion protein to the nucleus.

To determine which single amino acids may be critical for the nuclear localization of Tax, the subcellular localization of single amino acid mutants of GFP-Tax were examined (Table 1 and Fig. 1*B*). We focused on the zinc finger like motif between amino acids 23–52 and the basic amino acid cluster between 39–43, because these motifs are potential binding sites for importin β (23, 27, 28, 30, 48). Site directed mutagenesis of these amino acids were carried out. Among 20 mutants generated, 5 mutants (C29A, C36A, R42A, C49A, H52A) within the N-terminal 60 amino acids exhibited a dominant distribution in the cytoplasm (Table 1 and Fig. 1*B*). Taken together, our data confirm that the zinc finger motif within the N-terminal 60 amino acids is important for the nuclear localization of Tax.

Tax Enters the Nucleus by an Energy- and Carrier-independent Mechanism—To investigate the mechanisms by which Tax is transported into the nucleus, an *in vitro* nuclear import assay using digitonin-permeabilized cells was carried out (45).

Proteins larger than 40 kDa are generally transported through the NPC by an active and receptor-mediated mechanism (49). The import substrates used in these studies were full-length Tax, and the C-terminal deletion mutant Tax fused with GFP at their C terminus (Tax-GFP and Tax340-GFP) both of which are ~66 kDa in size and which would not be expected to enter the nucleus by a passive diffusion. GST-SV40TNLS-GFP was employed as a control carrier-dependent import substrate. In the complete assay system, which contained both cytosol and energy, all three substrates were efficiently imported into the nucleus (Fig. 2*A*, *panels a*, *d*, and *g*). Wheat germ agglutinin (WGA) binds to glycosylated nucleoporins and blocks nuclear transport mediated via the NPC (50, 51). In cells treated with WGA, none of the substrates accumulated in the nucleus (Fig. 2*A*, *panels b*, *e*, and *h*). Nuclear import was also inhibited by "on-ice" incubation (Fig. 2*A*, *panels c*, *f*, and *i*). These results indicate that the nuclear import of Tax-GFP and Tax340-GFP are carried out by an active transport mechanism through the active transport channels of the NPC, and not by passive diffusion.

TABLE 1
Subcellular localization of GFP-Tax with single amino acid mutation

Mutation	Subcellular localization
C23A	WT[a]
C29A	C[b]
C36A	C
R39A	WT
H41A	WT
R42A	C
H43A	WT
C49A	C
H52A	C
R62A	WT
R74A	WT
R82A	WT
K85A	WT
K88A	WT
R110A	WT
H127A	WT
C153A	WT
C174A	WT
R190A	WT

[a] WT, the localization of the mutant is similar to that of GFP with wild type Tax.
[b] C, the mutant localizes predominantly in the cytoplasm.

To further characterize the nuclear import of Tax, the effects of the depletion of energy or cytosol from import mixtures were examined. The depletion of energy markedly inhibited the nuclear import of GST-SV40TNLS-GFP but had no effect on the nuclear import of Tax-GFP and Tax340-GFP (Fig. 2*B*, *panels b*, *f*, and *j*). Interestingly, Tax340-GFP was imported into the nucleus even in the absence of cytosol. In contrast, Tax-GFP was found also to preferentially localize to the nuclear membrane and did not have such a clear cut distribution within the nucleus compared with the C-terminal deletion mutant (Fig. 2*B*, *panels c* and *g*). To investigate the effect of Ran on the nuclear import of Tax, RanQ69L, a mutant Ran which is deficient in GTP hydrolysis was added to the import mixture (Fig. 2*B*, *panels d*, *h*, and *l*). RanQ69L effectively inhibited the nuclear accumulation of GST-SV40TNLS-GFP, but not that of Tax-GFP and Tax340-GFP. These results indicate that Tax can enter the nucleus without energy or carriers including the importin β family proteins, which are known to require the GTPase activity of Ran for carrier function (23).

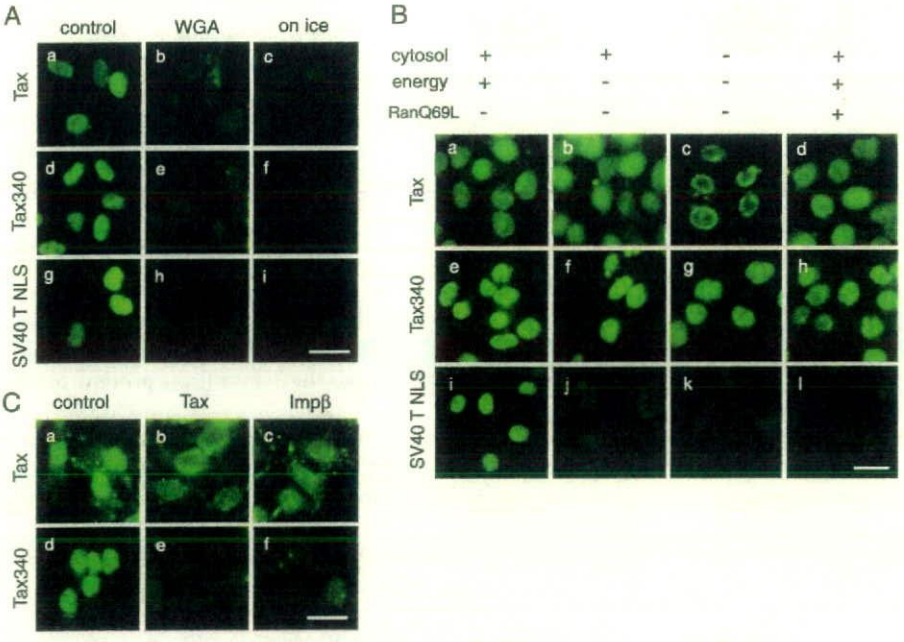

FIGURE 2. **The nuclear import of Tax is carried out by a facilitated process that is independent of energy and carriers.** The nuclear import of Tax-GFP (*Tax*), Tax340-GFP (*Tax340*), and GST-SV40TNLS-GFP (*SV40 T NLS*) were examined by *in vitro* nuclear import assay. *A*, digitonin-permeabilized HeLa cells were incubated with 10 μl of reaction mixtures containing 0.3 μM of an import substrate, ATP regeneration system, and rabbit reticulocyte lysate. Permeabilized cells were pretreated with 0.5 mg/ml WGA (Sigma) for 10 min at room temperature (*panels b*, *e* and *h*). The import reactions were performed at on ice instead of 30 °C (*panels c*, *f* and *i*). *B*, digitonin-permeabilized HeLa cells were incubated with 10 μl of reaction mixtures containing 0.3 μM of import substrate. To eliminate triphosphoric acids, the reaction mixtures were preincubated in the presence of 0.1 units/ml apyrase (Sigma) for 5 min at 30 °C prior to the reactions of energy-free conditions (*panels b*, *c*, *f*, *g*, *j*, and *k*). 5 μM RanQ69L-GTP were included in the reactions of the +*RanQ69L* condition (*panels d*, *h* and *i*). *C*, compositions of import mixtures were essentially as same as that of *A*, *panels a* and *d*. The import mixtures contained 30 μM GST (*control*, *panels a* and *d*), 30 μM GST-Tax (*Tax*, *panels b* and *e*), and 30 μM GST-importin β (*Impβ*, *panels c* and *f*) as competitors. *Scale bars*, 20 μm.

The Nuclear Import of Tax Involves a Direct Interaction with the FG Repeats of Nucleoporins—As it has been reported that the carrier-independent translocation of proteins into the nucleus involves a

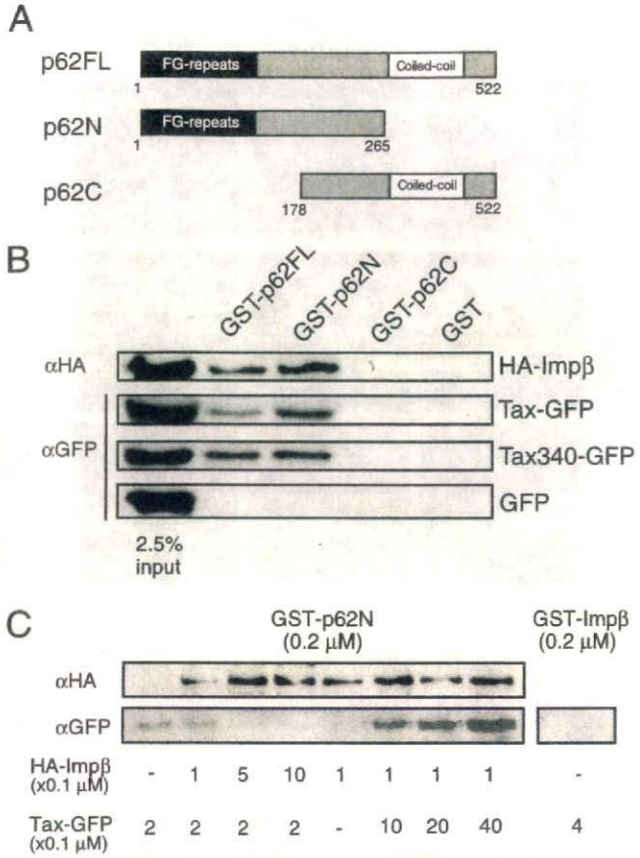

FIGURE 3. **Tax binds directly to the FG repeat region of p62 *in vitro*.** *A*, scheme of *p62FL* and its deletion mutants, *p62N* and *p62C*, which were used in the protein binding assay. *B* and *C*, in protein binding assays, the mixtures of recombinant proteins were allowed to immobilize on glutathione-Sepharose 4B beads, and bound fractions were analyzed by immunoblotting. In *B*, recombinant *GST*, *GST-p62FL*, *GST-p62N*, and *GST-p62C* (0.2 μM each) were mixed and incubated with *HA-Impβ*, *Tax-GFP*, *Tax340-GFP*, or *GFP* (0.2 μM each). To minimize the differences in the elution efficiencies between all GST fusion proteins from the beads, the total volume of the mixtures were increased to 300 μl, and the elution step was carried out three times. In *C*, recombinant GST-p62N was mixed and incubated at the indicated concentrations of *HA-Impβ* and *Tax-GFP*. *FL*, full-length. *Impβ*, importin β.

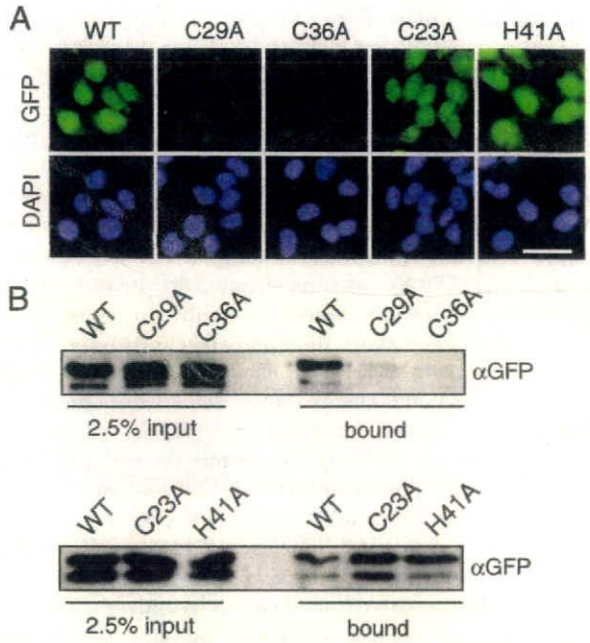

FIGURE 4. **The nuclear import activity of Tax is dependent on the binding of Tax and the FG repeats of nucleoporin.** The recombinant GFP fusions, Tax-GFP (*WT*), TaxC23A-GFP (*C23A*), TaxC29A-GFP (*C29A*), TaxC36A-GFP (*C36A*), and TaxH41A-GFP (*H41A*) were examined by *in vitro* nuclear import assay (*A*) and protein binding assay (*B*). In *A*, the digitonin-permeabilized HeLa cells were incubated with 10 μl of reaction mixtures containing 0.3 μM GFP fusions, ATP regeneration system, and RRL. *Scale bars*, 20 μm. In *B*, GST-p62N (0.2 μM) was mixed and incubated with GFP fusions (0.2 μM each). The reaction mixtures were then allowed to immobilize on glutathione-Sepharose 4B beads, and bound fractions were analyzed by immunoblotting using anti-GFP antibody.

direct interaction(s) between the proteins and nucleoporins within the NPC (23,35–38,52), we investigated whether Tax can also interact with nucleoporins. The FG repeat containing nucleoporins, including p62, Nup153, and Nup214/CAN have been implicated in nuclear import and are also known to interact with several importin β family proteins (reviewed in Ref. 53). To investigate if Tax can interact with nucleoporins, recombinant GST fused with full-length p62 and both C- or N-terminal deletion mutants of this protein were purified and assayed for their binding to Tax-GFP or HA-importin β. The C-terminal deletion mutant of p62 (p62N) contained the FG repeat region, whereas the N-terminal deletion mutant of p62 (p62C) did not (Fig. 3*A*). In control experiments, HA-importin β was found to bind to "full-length" GST-p62FL and to GST-p62N. This was also shown not to bind to GST-p62C or GST itself (Fig. 3*B*). Tax-GFP and Tax340-GFP also specifically bound to GST-p62FL and GST-p62N (Fig. 3*B*, right). Interactions of GFP and GST or GST fusion proteins were not observed. These results clearly show that Tax interacts with the FG repeat region of p62 *in vitro*. Our studies also suggest that Tax340 may bind p62FL with a greater affinity than wild type Tax (Fig. 3*B*). However this remains to be further investigated.

To determine if Tax and importin β compete for the binding to the FG repeats of p62, *in vitro* competition assays were carried out (Fig. 3*C*). Only a 2.5-fold amount of importin β effectively inhibited the binding between Tax and p62. In contrast, as much as a 40-fold amount of Tax did not completely inhibit the binding between importin β and p62. Binding between importin β and Tax was not observed (Fig. 3*C*, *right*). This suggests that Tax and importin β may share common docking sites on the FG repeats of nucleoporins, but the affinity between Tax and p62 is considerably lower than that between importin β and p62. To determine whether the nuclear import activity of Tax is dependent on an interaction between Tax and nucleoporins, the single amino acid Tax mutants, which were found to have lost (C29A and C36A) or retained (C23A and H41A) their nuclear localization properties (Fig. 1*B*), were expressed as GFP fusion proteins, and their nuclear import activity and binding affinity with p62 examined. Among wild type Tax and the four mutants, the nuclear import activities in digitonin-permeabilized cells closely correlated with the binding affinity with p62 (Fig. 4). Specifically these results support the proposal that the nuclear import of Tax requires direct interactions with regions in the nucleoporins containing the FG repeats.

The Nuclear Export of Tax Is Also Carrier- and Energy-independent—A number of studies have shown that certain proteins which enter the nucleus without import carriers (transportin, β-catenin, and MAPK) are also known to exit the nucleus without export carriers (35, 54–56). This raised the possibility that Tax may also exit from the nucleus without export carriers, and to investigate this, we examined the export of Tax using digitonin-permeabilized cells. Cells were firstly incubated with import mixtures containing Tax-GFP, Tax340-GFP, and GST-YFP-Rev as control, and subsequently washed and incubated with export buffer. To identify the components required for nuclear export, the export reactions were carried out with transport buffer (Fig. 5, *panels a*, *d*, and *g*) or buffer containing cytosol and energy (Fig. 5, *panels b*, *e*, and *h*). In addition, the transport buffer containing WGA was used to confirm the integrity of the nuclear membrane structures (Fig. 5, *panels c*, *f*, and *i*). The export of GST-YFP-Rev was observed only in the presence of cytosolic factors and energy, consistent with previous reports that the nuclear export of the HIV-1 Rev was CRM1-dependent (Fig. 5, *panel h*) (57). In contrast, GST-YFP-Rev was not exported from the nucleus under cytosol- and energy-free conditions (Fig. 5, *panel g*). Tax-GFP and Tax340-GFP were efficiently exported under the same conditions (Fig. 5, *panels a* and *d*). Quantification of the export process demonstrated that the export efficiencies of Tax-GFP and Tax340-GFP in the presence of cytosol and energy (Fig. 5, *panels b* and *e*) were almost the same as that in the absence of cytosol and energy (Fig. 5, *panels a* and *d*). These results indicate that Tax is also able to exit the nucleus in an energy- and carrier-independent manner.

Tax Can Transport p65 into the Nucleus—Our results have demonstrated that Tax can enter and exit the nucleus without a carrier protein, and these processes are energy-independent. Moreover, the nuclear import process appears to involve a direct interaction between Tax and the FG repeat regions of nucleoporins. Because these properties are also shared with known import receptors such as the importin β family proteins (58–61), we attempted to determine if Tax can also function as an import receptor. p65, an NF-κB family protein subunit, was chosen as a putative cargo of Tax, because this protein has been shown to be closely associated with Tax both in the cytoplasm and in the nucleus. Specifically, Tax has been associated with the release of p65 from the IκBα-p65 complex in the cytoplasm (13), and Tax and p65 co-localize in the nucleus (14). In addition, physical binding of Tax and p65 has been reported (62, 63). To determine whether p65 can be imported by Tax, p65 fused with YFP (p65-YFP) and Tax340 fused with CFP (Tax340-CFP) were expressed and used as substrates in the *in vitro* nuclear import assay. In the presence of energy and cytosol, p65-YFP was found to be distributed in both the nucleus and cytoplasm (Fig. 6*A*, *panel a*). The nuclear import of p65-YFP was inhibited by the addition of WGA or RanQ69L (Fig. 6*A*, *panels b* and *c*) and by the deprivation of cytosol in the import mixtures (Fig. 6*B*, *panel a*), all of which is consistent with the nuclear import of p65 being carried out by the importin α/β-mediated classical import pathway (64). Tax340-CFP was also expressed, and we confirmed as expected that the nuclear import of Tax340-CFP was a carrier- and an energy-independent process (data not shown). As shown in Fig. 6*B*, even without the addition of cytosolic factors and energy, p65-YFP was localized in the nucleus in the presence of Tax340. Moreover, p65-YFP migrated into the nucleus even in the presence of RanQ69L and cytosol if Tax-CFP was present in the import mixture (data not shown). These results indicate that p65 can migrate into the nucleus not only by the importin α/β import pathway, but also by a Tax-mediated pathway.

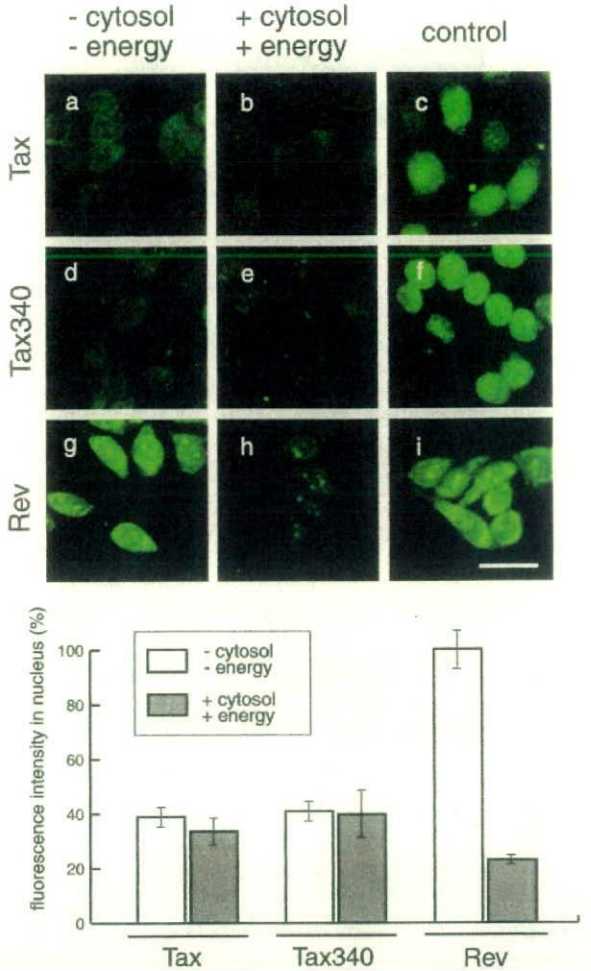

FIGURE 5. **Tax can be exported from the nucleus without carriers and energy.** The nuclear export of Tax-GFP (*Tax*), Tax340-GFP (*Tax340*), and GST-YFP-Rev (*Rev*) were examined. The digitonin-permeabilized HeLa cells were initially incubated with 10 μl of reaction mixtures containing import substrates (0.3 μM Tax-GFP, 0.3 μM Tax340-GFP, or 1.0 μM GST-YFP-Rev), RRL, and the ATP-regeneration system. Cells were then washed and reincubated with transport buffer (*−cytosol −energy*), that containing RRL and the ATP regeneration system (*+cytosol +energy*) or that containing 0.5 mg/ml WGA (*control*) to examine export. To obtain optimal nuclear accumulation of GST-YFP-Rev, all cells were pretreated with 10 nM leptomycin B for 30 min prior to digitonin permeabilization, and 10 nM leptomycin B was also included in the import reaction mixtures. *Graph*, fluorescent intensity of each nucleus was measured after the export reactions. The mean intensity of 30–40 nuclei was drawn. The mean intensity of nuclei incubated in the presence of 0.5 mg/ml WGA was taken as 100%. *Error bars* indicated standard deviation of the results of four independent experiments. *Scale bars*, 20 μm.

DISCUSSION

A number of studies have clearly shown that HTLV-1 Tax protein co-localizes in both the nucleus and the cytoplasm. In

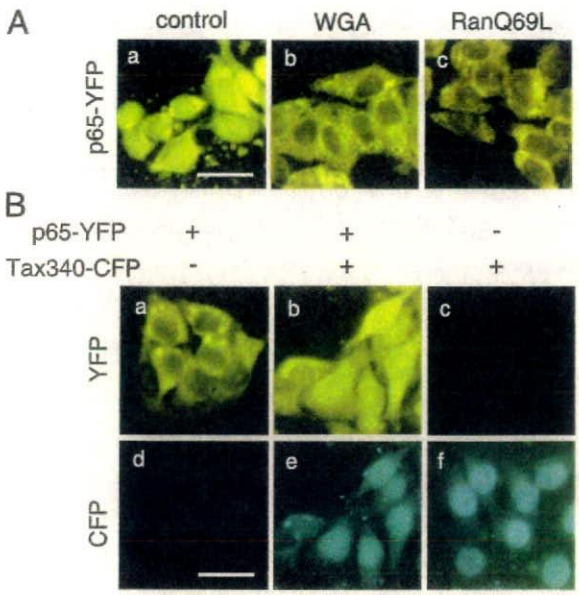

FIGURE 6. **p65 can be imported into the nucleus by Tax.** *A*, nuclear import of p65-YFP was characterized by *in vitro* nuclear import assay. Digitonin-permeabilized HeLa cells were incubated with 10 μl of standard import mixtures containing 0.2 μM p65-YFP, ATP regeneration system, and RRL (*panel a, control*). Before the incubation, permeabilized cells were pretreated with 0.5 mg/ml WGA (Sigma) for 10 min at room temperature (*panel b, WGA*). 5 μM RanQ69L-GTP was included in the standard import mixture (*panel c, RanQ69L*). *B*, the nuclear import of p65-YFP was examined in the absence of cytosol and energy. The import mixtures contained 0.2 μM p65-YFP under the *+p65-YFP* condition (*panels a, b, d,* and *e*), and 0.5 μM Tax340-CFP was under the *+Tax340-CFP* condition (*panels b, c, e,* and *f*). The import mixtures were pretreated with apyrase (0.1 unit/ml) prior to the import reactions. *Scale bars*, 20 μm.

the nucleus, Tax is observed in speckles in the so-called Tax speckle structure (TSS) where it is involved in the transcription of cellular genes through interactions with a number of transcription factors (14–16). In the cytoplasm, in addition to being directly involved with NF-κB activation (reviewed in Ref. 13), Tax co-localizes in several subcellular organelles including the endoplasmic reticulum, the Golgi apparatus, and the microtubule-organizing center (MTOC) and is believed to influence secretion pathways and microtubule organization (21, 22).

In the present study, we have investigated the intracellular localization of Tax and specifically the mechanisms involved in its nuclear localization. These have clearly shown that the nuclear import of Tax is carrier independent. Most proteins are transported into the nucleus by forming complexes with carrier proteins, which belong to importin β families with the carrier-cargo complex subsequently translocating through the NPC (23). However, a number of proteins have been shown to enter the nucleus directly. These include the carrier proteins themselves importin β (59), transportin (54), and importin α (65), as well as β-catenin (34), MAPK (35, 36), SMAD (37), STAT (38), HIV-1 Vpr (39), RCC1 (40) and PU.1 (41). We have also clearly shown that Tax requires neither energy nor Ran for its nuclear import which is a characteristic feature of proteins with a carrier-independent nuclear import (34, 35, 37, 39, 54). A common feature of the carrier-independent process is the direct interaction of proteins with nucleoporins in the NPC (23, 35–38, 41, 52). In the present study, we could also demonstrate a direct interaction between Tax and p62, one of the nucleoporins, which is located in the central plug of the NPC suggesting that Tax also shares this common property. It could be demonstrated using specific Tax mutants that the nuclear import of Tax correlated with the binding to p62 suggesting that this is an essential part of nuclear import. In addition, it could be shown that the nuclear import of Tax was inhibited by an excess amount of importin β, and that the binding between Tax and p62 was blocked by importin β. Taken together, the results suggest that Tax and importin β bind to a common region(s) in the nucleoporins.

Carrier- and energy-independent nuclear transport is thought to be carried out by a process similar to the so-called "facilitated diffusion," which requires specific, but weak interactions between the protein and nucleoporins (40, 66, 67). This sort of transport mechanism involves minimal energy and is thought to be driven by Brownian motion. In the case of β-catenin, the subcellular localization of the protein is thought to be controlled by retention in either the nucleus or the cytoplasm rather than a selective increase of import or export. Specifically, the transcription factors including T-cell factor/lymphocyte enhancer factor (LEF/TCF) and BCL9 or the cytoplasmic proteins including APC and Axin function as nuclear or cytoplasmic retention factors for β-catenin (68). The nuclear localization of MAPK is also thought to be regulated by the nuclear anchor proteins (69). Consistent with this, it is possible that the nuclear localization of Tax might be related to retention caused by Tax-binding proteins in the nucleus such as p65 and CBP, which serve as a bridge between the nucleosome and Tax. Cytoplasmic localization could involve immobile structures such as the MTOC and cytoskeleton to which Tax can bind directly or indirectly. One important observation in our study was that Tax340 was imported into the nucleus efficiently without cytosol and energy, but wild type Tax was imported efficiently only in the presence of cytosol. It is likely that the C-terminal 13 amino acids, which we have shown to be associated with the cytoplasmic distribution of Tax may serve as part of a "cytoplasmic retention signal." In the absence of cytosol, the C terminus of Tax could be sequestered by immobile structures in the cytoplasm, and in the presence of cytosol, Tax would be released from the cytoplasmic retention by the protein binding to the C terminus of Tax and permitting translocation through the NPC. It is also possible that Tax340 may have a greater binding affinity for the NPC compared with wild type Tax facilitating nuclear localization but this will require further detailed investigations. These and other studies are underway to further examine the importance of the C-terminal region in the localization of Tax.

The mechanisms of the nuclear export of Tax also remain to be defined. It was recently shown that under UV stress conditions, Tax was exported from the nucleus by an interaction with the carrier protein CRM1, on the basis that this was inhibited by leptomycin B (70). In contrast, under normal culture conditions, the nuclear export of Tax was found to be insensitive to leptomycin B (20, 70). As we demonstrated that the addition of exogenous transport factor and energy did not facilitate the nuclear export of Tax, it appears that Tax can exit the nucleus in a carrier and energy independent manner and this may account

for the report of the leptomycin B-insensitive nuclear export of Tax. Carrier-independent nuclear export has also been observed in a number of proteins, which have a carrier-independent nuclear import, such as transportin (54), MAPK (35), and β-catenin (55, 56).

It has recently been shown that β-catenin can also itself function as a carrier for the nuclear import of the LEF/TCF protein (71). This prompted us to investigate if Tax could also serve as a carrier for the import of cellular proteins. Several reports have demonstrated a direct interaction between Tax and the NF-κB subunit p65 (62, 63), and we could show that Tax functions as a nuclear import receptor for p65 at least under our *in vitro* conditions. Tax is known to have intimate interactions with p65 both in the cytoplasm and nucleus. Specifically, Tax is involved in the disassembly of the p65-IκBα complex in the cytoplasm (reviewed in Ref. 13) and co-localizes with p65 in the nucleus (14, 72). Therefore, we propose that p65 and Tax may form a complex in the cytoplasm, which can translocate to the nucleus through both a Tax carrier and an importin α/β-mediated mechanism. This proposal is supported by a recent study (62), where it was reported that the p65-CBP-Tax ternary complex is translocated into the nucleus immediately after its formation in the cytoplasm. Employing cellular fractionation studies, it could be shown that when p65, CBP and wild type Tax were co-transfected, the p65-CBP-Tax complex was located in the nucleus. In contrast, if p65, CBP and TaxΔ58, the NLS deletion mutant of Tax, were co-transfected, the p65-CBP-TaxΔ58 complex remained in the cytoplasm. These observations would support our hypothesis that Tax may function as an import receptor for this ternary complex.

With a carrier function, it might be expected that Tax could alter the normal nuclear/cytoplasmic distribution of cellular proteins by functioning as an exogenous transport receptor. Tax has been shown to bind with numerous cellular proteins, and fractionation of whole cell lysates from a HTLV-1-infected T cell line revealed that Tax is found in large protein complexes (~1800 kDa) *in vivo* (73). The ability of Tax to form protein complexes with cellular proteins together with a transport receptor-like function could lead to changes in the nucleo-cytoplasmic distribution of cellular proteins. Indeed, several Tax-binding proteins seem to be mistranslocated by Tax. Specifically, hsMAD1 is mistranslocated into the cytoplasm in the presence of Tax (74). More recently, a redistribution of IKKγ into the Golgi apparatus has been observed under Tax-expressing conditions (75). The disturbances of the nucleo-cytoplasmic transport pathway of host cellular proteins has been considered to be a strategy for survival of several viruses. For example, vesicular stomatitis virus, poliovirus, rhinovirus, and cardiovirus have been shown to induce abnormalities in the nucleo-cytoplasmic protein transport by affecting the structures of the NPC (76–78). Moreover, viral proteins of cytomegalovirus M50/p35 and the HIV-1 Vpr are known to cause the disruption of the nuclear envelope itself probably by the interacting with structural proteins of the nuclear envelope (79, 80). Our studies would suggest that Tax could cause significant nucleo-cytoplasmic traffic disturbances as a result of its import and possibly export receptor-like function. Continued studies are required to understand how this novel function of Tax may contribute to the pathogenesis of HTLV-1-related diseases.

Acknowledgments—We thank Dr. Y. Okada for technical advice and critical reading of the manuscript. We acknowledge Dr. S. Kose and Dr. N. Imamoto for kindly providing plasmids and helpful comments, and Dr. N. Yaseen and Dr. D. Dermot for kindly providing plasmids.

REFERENCES

1. Yoshida, M., Miyoshi, I., and Hinuma, Y. (1982) *Proc. Natl. Acad. Sci. U. S. A.* **79,** 2031–2035
2. Seiki, M., Hattori, S., Hirayama, Y., and Yoshida, M. (1983) *Proc. Natl. Acad. Sci. U. S. A.* **80,** 3618–3622
3. Grassmann, R., Dengler, C., Muller-Fleckenstein, I., Fleckenstein, B., McGuire, K., Dokhelar, M. C., Sodroski, J. G., and Haseltine, W. A. (1989) *Proc. Natl. Acad. Sci. U. S. A.* **86,** 3351–3355
4. Tanaka, A., Takahashi, C., Yamaoka, S., Nosaka, T., Maki, M., and Hatanaka, M. (1990) *Proc. Natl. Acad. Sci. U. S. A.* **87,** 1071–1075
5. Nerenberg, M., Hinrichs, S. H., Reynolds, R. K., Khoury, G., and Jay, G. (1987) *Science* **237,** 1324–1329
6. Grossman, W. J., Kimata, J. T., Wong, F. H., Zutter, M., Ley, T. J., and Ratner, L. (1995) *Proc. Natl. Acad. Sci. U. S. A.* **92,** 1057–1061
7. Yamada, S., Ikeda, H., Yamazaki, H., Shikishima, H., Kikuchi, K., Wakisaka, A., Kasai, N., Shimotohno, K., and Yoshiki, T. (1995) *Cancer Res.* **55,** 2524–2527
8. Hasegawa, H., Sawa, H., Lewis, M. J., Orba, Y., Sheehy, N., Yamamoto, Y., Ichinohe, T., Tsunetsugu-Yokota, Y., Katano, H., Takahashi, H., Matsuda, J., Sata, T., Kurata, T., Nagashima, K., and Hall, W. W. (2006) *Nat. Med.* **12,** 466–472
9. Matsuoka, M. (2003) *Oncogene* **22,** 5131–5140
10. Yoshida, M. (2001) *Annu. Rev. Immunol.* **19,** 475–496
11. Jeang, K. T., Giam, C. Z., Majone, F., and Aboud, M. (2004) *J. Biol. Chem.* **279,** 31991–31994
12. Sun, S. C., and Yamaoka, S. (2005) *Oncogene* **24,** 5952–5964
13. Peloponese, J. M., Yeung, M. L., and Jeang, K. T. (2006) *Immunol. Res.* **34,** 1–12
14. Bex, F., McDowall, A., Burny, A., and Gaynor, R. (1997) *J. Virol.* **71,** 3484–3497
15. Bex, F., Yin, M. J., Burny, A., and Gaynor, R. B. (1998) *Mol. Cell. Biol.* **18,** 2392–2405
16. Semmes, O. J., and Jeang, K. T. (1996) *J. Virol.* **70,** 6347–6357
17. Nicot, C., Tie, F., and Giam, C. Z. (1998) *J. Virol.* **72,** 6777–6784
18. Burton, M., Upadhyaya, C. D., Maier, B., Hope, T. J., and Semmes, O. J. (2000) *J. Virol.* **74,** 2351–2364
19. Cheng, H., Cenciarelli, C., Shao, Z., Vidal, M., Parks, W. P., Pagano, M., and Cheng-Mayer, C. (2001) *Curr. Biol.* **11,** 1771–1775
20. Alefantis, T., Barmak, K., Harhaj, E. W., Grant, C., and Wigdahl, B. (2003) *J. Biol. Chem.* **278,** 21814–21822
21. Alefantis, T., Mostoller, K., Jain, P., Harhaj, E., Grant, C., and Wigdahl, B. (2005) *J. Biol. Chem.* **280,** 17353–17362
22. Nejmeddine, M., Barnard, A. L., Tanaka, Y., Taylor, G. P., and Bangham, C. R. (2005) *J. Biol. Chem.* **280,** 29653–29660
23. Harel, A., and Forbes, D. J. (2004) *Mol Cell.* **16,** 319–330
24. Pemberton, L. F., and Paschal, B. M. (2005) *Traffic* **6,** 187–198
25. Lam, M. H., Thomas, R. J., Loveland, K. L., Schilders, S., Gu, M., Martin, T. J., Gillespie, M. T., and Jans, D. A. (2002) *Mol. Endocrinol.* **16,** 390–401
26. Nagoshi, E., Imamoto, N., Sato, R., and Yoneda, Y. (1999) *Mol. Biol. Cell* **10,** 2221–2233
27. Yamasaki, H., Sekimoto, T., Ohkubo, T., Douchi, T., Nagata, Y., Ozawa, M., and Yoneda, Y. (2005) *Genes Cells* **10,** 455–464
28. Truant, R., and Cullen, B. R. (1999) *Mol. Cell. Biol.* **19,** 1210–1217
29. Arnold, M., Nath, A., Hauber, J., and Kehlenbach, R. H. (2006) *J. Biol. Chem.* **281,** 20883–20890
30. Palmeri, D., and Malim, M. H. (1999) *Mol. Cell. Biol.* **19,** 1218–1225
31. Pollard, V. W., Michael, W. M., Nakielny, S., Siomi, M. C., Wang, F., and Dreyfuss, G. (1996) *Cell* **86,** 985–994

32. Baake, M., Bauerle, M., Doenecke, D., and Albig, W. (2001) *Eur. J. Cell Biol.* **80,** 669–677
33. Jakel, S., and Gorlich, D. (1998) *EMBO J.* **17,** 4491–4502
34. Yokoya, F., Imamoto, N., Tachibana, T., and Yoneda, Y. (1999) *Mol. Biol. Cell.* **10,** 1119–1131
35. Matsubayashi, Y., Fukuda, M., and Nishida, E. (2001) *J. Biol. Chem.* **276,** 41755–41760
36. Whitehurst, A. W., Wilsbacher, J. L., You, Y., Luby-Phelps, K., Moore, M. S., and Cobb, M. H. (2002) *Proc. Natl. Acad. Sci. U. S. A.* **99,** 7496–7501
37. Xu, L., Alarcon, C., Col, S., and Massague, J. (2003) *J. Biol. Chem.* **278,** 42569–42577
38. Marg, A., Shan, Y., Meyer, T., Meissner, T., Brandenburg, M., and Vinkemeier, U. (2004) *J. Cell Biol.* **165,** 823–833
39. Jenkins, Y., McEntee, M., Weis, K., and Greene, W. C. (1998) *J. Cell Biol.* **143,** 875–885
40. Nemergut, M. E., and Macara, I. G. (2000) *J. Cell Biol.* **149,** 835–850
41. Zhong, H., Takeda, A., Nazari, R., Shio, H., Blobel, G., and Yaseen, N. R. (2005) *J. Biol. Chem.* **280,** 10675–10682
42. Smith, M. R., and Greene, W. C. (1992) *Virology* **187,** 316–320
43. Smith, M. R., and Greene, W. C. (1990) *Genes Dev.* **4,** 1875–1885
44. Gitlin, S. D., Lindholm, P. F., Marriott, S. J., and Brady, J. N. (1991) *J. Virol.* **65,** 2612–2621
45. Adam, S. A., Marr, R. S., and Gerace, L. (1990) *J. Cell Biol.* **111,** 807–816
46. Semmes, O. J., and Jeang, K. T. (1992) *J. Virol.* **66,** 7183–7192
47. Meertens, L., Chevalier, S., Weil, R., Gessain, A., and Mahieux, R. (2004) *J. Biol. Chem.* **279,** 43307–43320
48. Pandya, K., and Townes, T. M. (2002) *J. Biol. Chem.* **277,** 16304–16312
49. Gorlich, D. (1998) *EMBO J.* **17,** 2721–2727
50. Finlay, D. R., Newmeyer, D. D., Price, T. M., and Forbes, D. J. (1987) *J. Cell Biol.* **104,** 189–200
51. Yoneda, Y., Imamoto-Sonobe, N., Yamaizumi, M., and Uchida, T. (1987) *Exp. Cell Res.* **173,** 586–595
52. Vodicka, M. A., Koepp, D. M., Silver, P. A., and Emerman, M. (1998) *Genes Dev.* **12,** 175–185
53. Ryan, K. J., and Wente, S. R. (2000) *Curr. Opin. Cell Biol.* **12,** 361–371
54. Nakielny, S., and Dreyfuss, G. (1998) *Curr. Biol.* **8,** 89–95
55. Wiechens, N., and Fagotto, F. (2001) *Curr. Biol.* **11,** 18–27
56. Koike, M., Kose, S., Furuta, M., Taniguchi, N., Yokoya, F., Yoneda, Y., and Imamoto, N. (2004) *J. Biol. Chem.* **279,** 34038–34047
57. Fornerod, M., Ohno, M., Yoshida, M., and Mattaj, I. W. (1997) *Cell* **90,** 1051–1060
58. Ribbeck, K., Kutay, U., Paraskeva, E., and Gorlich, D. (1999) *Curr. Biol.* **9,** 47–50
59. Kose, S., Imamoto, N., Tachibana, T., Shimamoto, T., and Yoneda, Y. (1997) *J. Cell Biol.* **139,** 841–849
60. Englmeier, L., Olivo, J. C., and Mattaj, I. W. (1999) *Curr. Biol.* **9,** 30–41
61. Stewart, M. (2003) *Science* **302,** 1513–1514
62. Azran, I., Jeang, K. T., and Aboud, M. (2005) *Oncogene.* **24,** 4521–4530
63. Suzuki, T., Hirai, H., and Yoshida, M. (1994) *Oncogene.* **9,** 3099–3105
64. Fagerlund, R., Kinnunen, L., Kohler, M., Julkunen, I., and Melen, K. (2005) *J. Biol. Chem.* **280,** 15942–15951
65. Miyamoto, Y., Hieda, M., Harreman, M. T., Fukumoto, M., Saiwaki, T., Hodel, A. E., Corbett, A. H., and Yoneda, Y. (2002) *EMBO J.* **21,** 5833–5842
66. Wente, S. R. (2000) *Science* **288,** 1374–1377
67. Talcott, B., and Moore, M. S. (1999) *Trends Cell Biol.* **9,** 312–318
68. Krieghoff, E., Behrens, J., and Mayr, B. (2006) *J. Cell Sci.* **119,** 1453–14563
69. Lenormand, P., Brondello, J. M., Brunet, A., and Pouyssegur, J. (1998) *J. Cell Biol.* **142,** 625–633
70. Gatza, M. L., and Marriott, S. J. (2006) *J. Virol.* **80,** 6657–6668
71. Asally, M., and Yoneda, Y. (2005) *Exp. Cell Res.* **308,** 357–363
72. Nasr, R., Chiari, E., El Sabban, M., Mahieux, R., Kfoury, Y., Abdulhay, M., Yazbeck, V., Hermine, O., de The, H., Pique, C., and Bazarbachi, A. (2006) *Blood* **107,** 4021–4029
73. Wu, K., Bottazzi, M. E., de la Fuente, C., Deng, L., Gitlin, S. D., Maddukuri, A., Dadgar, S., Li, H., Vertes, A., Pumfery, A., and Kashanchi, F. (2004) *J. Biol. Chem.* **279,** 495–508
74. Kasai, T., Iwanaga, Y., Iha, H., and Jeang, K. T. (2002) *J. Biol. Chem.* **277,** 5187–5193
75. Harhaj, N. S., Sun, S. C., and Harhaj, E. W. (2006) *J. Biol. Chem.* **282,** 4185–4192
76. Feldherr, C., and Akin, D. (1995) *Mol. Cell. Biol.* **15,** 7043–7049
77. Delhaye, S., van Pesch, V., and Michiels, T. (2004) *J. Virol.* **78,** 4357–4362
78. Gustin, K. E. (2003) *Virus Res.* **95,** 35–44
79. Muranyi, W., Haas, J., Wagner, M., Krohne, G., and Koszinowski, U. H. (2002) *Science* **297,** 854–857
80. de Noronha, C. M., Sherman, M. P., Lin, H. W., Cavrois, M. V., Moir, R. D., Goldman, R. D., and Greene, W. C. (2001) *Science* **294,** 1105–1108

Overexpressed NF-κB–inducing kinase contributes to the tumorigenesis of adult T-cell leukemia and Hodgkin Reed-Sternberg cells

Yasunori Saitoh,[1] Norio Yamamoto,[1] M. Zahidunnabi Dewan,[1] Haruyo Sugimoto,[1] Vicente J. Martinez Bruyn,[1] Yuki Iwasaki,[1] Katsuyoshi Matsubara,[1] Xiaohua Qi,[1] Tatsuya Saitoh,[2] Issei Imoto,[3] Johji Inazawa,[3] Atae Utsunomiya,[4] Toshiki Watanabe,[5] Takao Masuda,[6] Naoki Yamamoto,[1,7] and Shoji Yamaoka[1]

[1]Department of Molecular Virology, Graduate School of Medicine, Tokyo Medical and Dental University, Tokyo; [2]Department of Host Defense, Research Institute for Microbial Diseases, Osaka University, Suita; [3]Department of Molecular Cytogenetics, Medical Research Institute and School of Biomedical Science, Tokyo Medical and Dental University, Tokyo; [4]Department of Hematology, Imamura Bun-in Hospital, Kagoshima; [5]Department of Medical Genome Sciences, Graduate School of Frontier Sciences, University of Tokyo, Tokyo; [6]Department of Immunotherapeutics, Graduate School of Medicine, Tokyo Medical and Dental University, Tokyo; and [7]AIDS Research Center, National Institute of Infectious Diseases, Tokyo, Japan

The nuclear factor-κB (NF-κB) transcription factors play important roles in cancer development by preventing apoptosis and facilitating the tumor cell growth. However, the precise mechanisms by which NF-κB is constitutively activated in specific cancer cells remain largely unknown. In our current study, we now report that NF-κB–inducing kinase (NIK) is overexpressed at the pretranslational level in adult T-cell leukemia (ATL) and Hodgkin Reed-Sternberg cells (H-RS) that do not express viral regulatory proteins. The overexpression of NIK causes cell transformation in rat fibroblasts, which is abolished by a super-repressor form of IκBα. Notably, depletion of NIK in ATL cells by RNA interference reduces the DNA-binding activity of NF-κB and NF-κB–dependent transcriptional activity, and efficiently suppresses tumor growth in NOD/SCID/γc^{null} mice. These results indicate that the deregulated expression of NIK plays a critical role in constitutive NF-κB activation in ATL and H-RS cells, and suggest also that NIK is an attractive molecular target for cancer therapy. (Blood. 2008;111:5118-5129)

Introduction

The nuclear factor-κB (NF-κB) transcription factors are known to regulate the expression of a wide range of genes involved in development, immune responses, apoptosis, and carcinogenesis as dimers of the REL family members, RelA, RelB, c-Rel, p50, and p52.[1] The p50 and p52 proteins are generated by proteasome-mediated processing of their precursors, p105 and p100, respectively. In resting cells, Rel proteins are sequestered in the cytoplasm through their interactions with the ankyrin repeats of the inhibitory proteins IκBα, -β, and -ε, as well as the precursor proteins p105 and p100. On stimulation, signals converge at the multiprotein IκB kinase (IKK) complex, which is composed of 2 catalytic subunits, IKK1/α and IKK2/β, and the scaffolding proteins, NF-κB essential modulator (NEMO, also known as IKKγ) and ELKS.[2] Phosphorylation by the IKK complex of specific serine residues on the IκB or precursor proteins results in their poly-ubiquitination and proteasome-dependent degradation or processing.[2] Released NF-κB then translocates to the nucleus and regulates expression of target genes.

NF-κB signaling pathways are largely classified as either canonical or noncanonical based on the stimuli and targets of the IKK complex.[2] Canonical activation is induced by stimuli, such as tumor necrosis factor-α (TNFα) and interleukin-1β, and involves NEMO- and IKK2/β-dependent phosphorylation and the subsequent degradation of IκB proteins. Noncanonical NF-κB pathways are activated after the stimulation of a range of TNF receptor family members, such as B-cell activating factor belonging to the TNF family (BAFF) receptor, lymphotoxin-β receptor, Fn14 and CD40, and direct NF-κB–inducing kinase (NIK)- and IKK1/α-dependent phosphorylation and subsequent processing of p100, leading to activation of NF-κB complexes containing RelB.[2,3] Of note in this context, the noncanonical pathways operate in a delayed fashion and are sensitive to protein synthesis inhibition.[4,5]

Compared with the mechanisms underlying the transduction of ligand-induced signaling to NF-κB activation, much less is known about how NF-κB is constitutively activated in a variety of cancer cells.[6] Constitutively high NF-κB activity has typically been demonstrated in human hematopoietic cancer cells, including adult T-cell leukemia (ATL), Hodgkin lymphoma, and multiple myeloma cells.[7,8] We have previously reported the aberrant expression of p52 in ATL and Hodgkin Reed-Sternberg (H-RS) cells that do not express viral regulatory proteins, such as Tax of the human T-cell leukemia virus or latent membrane protein 1 of the Epstein-Barr virus.[9,10] In addition, IKK activation in ATL and H-RS cells was found to be sensitive to protein synthesis inhibition.[10,11] These results indicate that the noncanonical pathways of NF-κB activation operate in these cancer cells. Aberrant p52 expression has also been reported in other types of cancer cells, including breast,[12] prostate,[13] pancreas,[14] and colon.[15] However, the actual triggers of noncanonical NF-κB activation in these cancer cells remain largely unknown except for certain multiple myeloma cells that have mutations in the *NIK*, *TRAF3*, and related genes.[16,17]

Submitted September 10, 2007; accepted February 17, 2008. Prepublished online as *Blood* First Edition paper, February 27, 2008; DOI 10.1182/blood-2007-09-110635.

The online version of this article contains a data supplement.

The publication costs of this article were defrayed in part by page charge payment. Therefore, and solely to indicate this fact, this article is hereby marked "advertisement" in accordance with 18 USC section 1734.

NIK is a serine-threonine kinase that is an essential participant in the induction of the IKK1-dependent processing of p100 as well as IκB degradation in response to stimuli, such as CD70, CD40 ligand, and BAFF.[18] It has also been reported previously that the IKK complex is recruited to CD27 in a manner dependent on NIK function. However, the mechanism by which NIK activity is regulated thereafter was unknown until it was recently demonstrated that these stimuli protect basally translated endogenous NIK protein from proteasome-mediated degradation.[19,20] Liao et al reported that the interaction of NIK with TNF receptor–associated factor 3 (TRAF3) is responsible for the rapid degradation of NIK and that noncanonical NF-κB stimuli induce the degradation of TRAF3 and the elevation of NIK expression.[19] In a separate study, Qing et al have demonstrated that noncanonical NF-κB stimuli stabilize the NIK protein but do not modify its RNA expression or protein translation.[20] The findings of these studies explain the delay in triggering the noncanonical pathway and its high sensitivity to protein synthesis inhibition.

Because NIK is a central regulator of the noncanonical pathway of NF-κB activation, we have investigated in our current study how this kinase is regulated in hematopoietic cancer cells, in which IKK is constitutively activated in the absence of viral regulators.

Methods

Cell culture

ED40515(−),[21] ATL-43Tb(−),[22] and TL-Om1[23] are human T-cell leukemia virus type-I (HTLV-I)–infected T-cell lines established from the leukemic cells of ATL patients. The H-RS cell lines, HDLM-2, L428, and L540, were purchased from the German Collection of Micro-organisms and Cell Cultures (Braunschweig, Germany). CEM[24] and Jurkat[25] are HTLV-I–free human T-lymphoblastic leukemia cell lines. A human B-cell line, Romas RG69,[20] was a kind gift from Dr Gutian Xiao (State University of New Jersey, Piscataway, NJ). Primary leukemia cells derived from ATL patients were obtained under informed consent at Imamura Bun-in Hospital and supplied through the Joint Study on Predisposing Factors of ATL Development. The patients were diagnosed with ATL on the basis of clinical and hematologic features and the presence of antibodies to ATL-associated antigens in serum and of the HTLV-I proviral genome in the leukemia cells. Use of peripheral blood lymphocytes from ATL patients for research purposes was approved by the institutional review board of each institute. Peripheral blood mononuclear cells (PBMCs) derived from healthy donors were also obtained under informed consent. PBMCs were isolated from both ATL patients and healthy donors by density gradient separation with Ficoll-Plaque PLUS (Amersham Biosciences, Uppsala, Sweden). Cells were maintained in RPMI 1640 supplemented with 10% fetal bovine serum, 100 U/mL penicillin G, and 100 μg/mL streptomycin sulfate; 5R is a NEMO-deficient subline of the Rat-1 cell line and has been described previously.[26] B5 and h12 are sublines of Rat-1 and 5R, respectively, express the blasticidin deaminase gene under the control of an NF-κB–dependent promoter, and have also been described previously.[26,27] Plat-E packaging cells were described previously.[28] B5, h12, Plat-E, 293T cells, and mouse embryonic fibroblasts were maintained in Dulbecco modified Eagle medium supplemented with 10% fetal bovine serum, 100 U/mL penicillin G, and 100 μg/mL streptomycin sulfate. Anchorage-independent cell growth was examined essentially as described previously.[29] Images were captured using an inverted microscope (IX70, Olympus, Tokyo, Japan) and processed with Openlab 3.0.2 software (Improvision, Coventry, United Kingdom). Cells used in this study were all maintained at 37°C in air containing 5% CO_2.

Virus infection and transfection

Plat-E cells were transfected with pMRX-HA-NIK-ires-puro, pMRX-HA-kd-NIK-ires-puro, or pMRX-HA-ires-puro (EV1) (Document S1, available on the *Blood* website; see the Supplemental Materials link at the top of the online article) using the calcium phosphate precipitation method. Culture supernatants were collected 48 hours after transfection and filtered. B5 and h12 cells were infected for 2 hours in the presence of 10 μg/mL polybrene. Infected cells were then cultured in medium containing 2 μg/mL puromycin, and cell clones were isolated. Rat fibroblasts expressing SR-IκBα or its empty control vector (EV2) were established essentially as described previously.[10] For production of lentiviruses, 293T cells were cotransfected with pCS-puro-Ctli, pCS-puro-NIKi-1, or pCS-puro-NIKi-2 (Document S1) together with the pCMVΔR8.2 packaging construct and pHCMV-VSV-G (kind gifts from Dr I.S.Y. Chen) using FuGENE 6 (Roche Applied Science, Indianapolis, IN). Culture supernatants were collected 48 hours after transfection and filtered. ED40515(−) and ATL-43Tb(−) cells were infected once or twice with 24 hours interval with these lentiviruses for 6 hours in the presence of 10 μg/mL polybrene. At 48 hours after the infection, cells were cultured in medium containing 2 μg/mL puromycin for an additional 48 hours. These infectants were subjected to immunoblotting, electrophoretic mobility shift assay (EMSA), and transient transfection with 2 μg of IgκCona-luc[30] and pEF1-LacZ[26] using DMRIE-C (Invitrogen, Carlsbad, CA) according to the manufacturer's instructions. Assays for luciferase and β-galactosidase were performed 48 hours after transfection by standard methods. Luciferase activity was normalized on the basis of β-galactosidase activity. The growth of lentivirus-infected cells was determined by the trypan blue staining method.

Immunoprecipitation

For the immunoprecipitation of endogenous NIK, approximately 2×10^7 cells were lysed in buffer A (20 mM Tris-HCl, pH7.5, 0.5% Nonidet P-40, 150 mM NaCl supplemented with 1 μg/mL aprotinin, 1 μg/mL leupeptin, 0.57 mM phenylmethanesulphonylfluoride, 10 μM MG132, 10 μM MG115) followed by preclearing with purified rabbit IgG (Cedarlane Laboratories, Hornby, ON) and protein G-Sepharose beads (Pierce Biotechnology, Rockford, IL). After centrifugation at 14000 rpm for 3 minutes, supernatants were subjected to immunoprecipitation with purified nonimmune rabbit IgG or anti-NIK antibody (#4994) (Cell Signaling Technology, Danvers, MA). Immunoprecipitates were washed 3 times with TNT buffer (20 mM Tris-HCl, pH 7.5, 200 mM NaCl, and 1% Triton X-100). Endogenous NIK proteins were detected by immunoblotting with anti-NIK antibody (#4994). For the immunoprecipitation of HA-tagged NIK, 750 μg cell lysates prepared with buffer A was subjected to immunoprecipitation with anti-HA antibody (12CA5, a kind gift from Dr A. Israël, Institut Pasteur Paris, Paris, France). Immunoprecipitates were washed 3 times with TNT buffer. HA-tagged NIK proteins were detected by immunoblotting with anti-NIK antibody. For immunoprecipitation of endogenous IKK1/2, 1500 μg cell lysates prepared with buffer A were subjected to immunoprecipitation with anti-IKK1 monoclonal antibody (B78-1; BD PharMingen, San Diego, CA) or purified mouse IgG2b (M110-104; Bethyl Laboratories, Montgomery, TX). Immunoprecipitates were washed 3 times with TNT buffer. Expression of endogenous proteins was detected by immunoblotting with antiphospho-IKK1/IKK2 (Ser180/Ser181) (#2681; Cell Signaling Technology), anti-IKK1 (H-744), or anti-IKK2 (H-470; Santa Cruz Biotechnology, Santa Cruz, CA) antibodies.

Quantitative RT-PCR

Total RNA was extracted using Isogen reagents (Nippon Gene, Tokyo, Japan) according to the manufacturer's instructions. Quantitative RT-PCR amplifications were performed with 100 ng total RNA, 0.3 μM of each primer, and 0.25 μM TaqMan probe using an ABI-7700 Sequence Detector (Applied Biosystems, Foster City, CA): reverse transcription was performed at 48°C for 30 minutes, Taq DNA polymerase was activated at 95°C for 10 minutes, followed by 45 amplification cycles of 95°C for 15 seconds, and annealing and extension at 60°C for 1 minute. The *NIK*, *VEGF*, *ICAM-1*, and *MMP-9* mRNA levels were normalized based on the amount of *18S* ribosomal RNA determined simultaneously by the real-time RT-PCR.

Mice and inoculation of cells

NOD/SCID/γc^{null} (NOG)[31] mice were purchased from the Central Institute for Experimental Animals (Kawasaki, Japan). All mice were maintained under specific pathogen-free conditions in the Animal Center of Tokyo Medical and Dental University (Tokyo, Japan). The Ethical Review Committee of the institute approved the experimental protocol. ED40515(−) cells expressing Ctli or NIKi-1 and -2 were washed twice with serum-free RPMI 1640 and resuspended in the same medium. Mice were anesthetized with ether and inoculated subcutaneously in the postauricular region with 5×10^6 cells per mouse, as described previously.[31] We measured tumor size and weight 2 weeks after cell inoculation.

Statistics

Statistical significance was evaluated using a 2-tailed, unpaired Student's *t* test. *P* values less than .05 were considered to be significant.

Results

NIK is aberrantly expressed in both adult T-cell leukemia and Hodgkin Reed-Sternberg cells

The constitutive processing of p100 to p52 in ATL and H-RS cells[9,10] prompted us to examine whether NIK is aberrantly expressed in both established and primary ATL cells. Immunoblotting of whole-cell lysates prepared from ATL or H-RS cells did not show any detectable NIK signal (data not shown); however, when endogenous NIK was immunoprecipitated from approximately 20 million of these cells and subjected to immunoblotting, NIK was specifically detectable in anti-NIK immunoprecipitates from ATL and H-RS cells, but not from control cells, such as CEM and Jurkat (Figure 1A). Previous studies revealed that inhibition of the proteasome function allowed for detection of endogenous NIK in simple whole-cell lysates of B-cell lines.[19,20] Treatment of ED-40515(−) cells with the MG132 proteasome inhibitor for 3 hours before harvesting enabled us to observe robust endogenous NIK expression at the expected position (Figure 1B). Lysates of 293T cells with or without exogenous NIK expression were used as the positive and negative controls, respectively. We next examined the NIK expression levels as well as those of p100 phosphorylated at serine residues 866 and 870 in a panel of ATL, H-RS, and control cells (Figure 1C). No appreciable NIK expression could be observed in control CEM and Jurkat T-cell lines treated with MG132, in which NF-κB is not constitutively activated. Proteasome inhibition induced strong NIK expression in other Tax-negative ATL-derived cell lines, ATL-43Tb(−) and TL-Om1. Proteasome inhibition also strongly augmented NIK expression in H-RS cells, but only weakly so in the control B-cell lines, RG69. These results indicate that the steady-state levels of NIK of the authentic size are elevated in ATL and H-RS cells, and suggest that NIK may be abundantly produced in ATL and H-RS cells, but is rapidly degraded by the proteasome. The levels of NIK expression correlated well with those of phosphorylated p100 (Figure 1C). Moreover, p52 and the phoshorylated form of IκBα were also abundant in ATL and H-RS cell lines, but not in the control T-cell lines (Figure 1C). These results indicate that the overexpression of NIK is closely linked to the downstream events leading to constitutive activation of the canonical and noncanonical NF-κB pathways in ATL and H-RS cells. A previous study suggested that L428 cells express a C-terminally truncated form of IκBα and that the phosphorylated form of this protein was accumulated after treatment of the cells with proteasome inhibitor or dexamethasone.[32,33] In agreement with this, we did not detect IκBα expression with the antibody used in this study, which recognizes the C-terminus of the protein, but detected the phoshorylated form of this IκBα only after treatment with MG132 (data not shown).

We next investigated *NIK* expression at the mRNA level by quantitative PCR (Figure 1D) and found that that *NIK* transcripts were at between 20- and 100-fold higher levels in ATL and H-RS cells, compared with CEM cells. Next, actinomycin D was used to block new mRNA synthesis, so that decay of existing transcripts could be detected. Quantitative PCR analyses revealed that the half-life of *NIK* mRNA was approximately 3 hours both in the ATL and control T cells (Figure 1E). Essentially similar results were obtained with the other cell lines shown in Figure 1D, including H-RS cell lines (data not shown). A previous report has demonstrated that NF-κB is constitutively activated in primary ATL cells in the peripheral blood.[34] We therefore quantified the *NIK* mRNA levels in PBMCs from both healthy donors and ATL patients (Figure 2A), and found that *NIK* mRNA is overexpressed in PBMCs of 15 of 21 ATL patients. Actinomycin D treatment of PBMCs further revealed that *NIK* mRNA was not apparently stabilized in primary ATL cells (Figure 2B). Moreover, fluorescence in situ hybridization studies on primary ATL cells failed to detect amplification or translocation of the *NIK* gene (Figure S1; Table S2). Finally, when PBMCs were cultured for 3 hours in the presence of MG132, NIK protein was detectable in cells from an ATL patient showing abundant *NIK* mRNA expression, but not in those from a healthy donor (Figure 2C).

NIK transforms rat fibroblasts in an NF-κB–dependent manner

To further explore the roles for NIK during cell transformation, we infected the 3T3-like rat fibroblast cell line Rat-1 with a retroviral vector expressing human NIK and examined its oncogenic activity. As expected, cells transduced with this NIK vector exhibited strong NF-κB DNA binding activity within 36 hours (data not shown). Rat-1 cells transduced with a control retrovirus became resistant to the selection marker puromycin approximately 24 hours after infection and continued to proliferate rapidly. In contrast, Rat-1 cells transduced with the NIK expression vector expressed a readily detectable level of NIK, had a transformed morphology, but ceased proliferating and died within 3 to 4 days after becoming resistant to puromycin. Cells that survived 2 weeks of puromycin selection after NIK transduction eventually appeared indistinguishable from those transduced with the control vector and showed no detectable NIK expression or NF-κB DNA binding activity (data not shown).

Based on these observations, we speculate that the retroviral overexpression of NIK is toxic to the cells so that only cells that had lost its expression could emerge from the puromycin-resistant pools. To address this problem, we used B5 and h12 cells carrying an integrated Igκ2bsrH plasmid that confers resistance to the antibiotic blasticidin S when cells are constitutively expressing active NF-κB.[26] B5 cells are derived from Rat-1 cells, and h12 cells are from 5R cells that lack NEMO expression. When the B5 and h12 cells were transduced with the wild-type NIK retroviral expression vector and subjected to selection with both puromycin and blasticidin S, the majority of the resultant cell clones maintained detectable NIK expression (Figure 3A), elevated catalytic activity of IKK (Figure 4), and the initial transformed morphology (Figure 5B). On the other hand, when B5 and h12 cells were transduced with a retrovirus vector expressing a catalytically inactive mutant form of NIK and selected with puromycin alone, the cells successfully

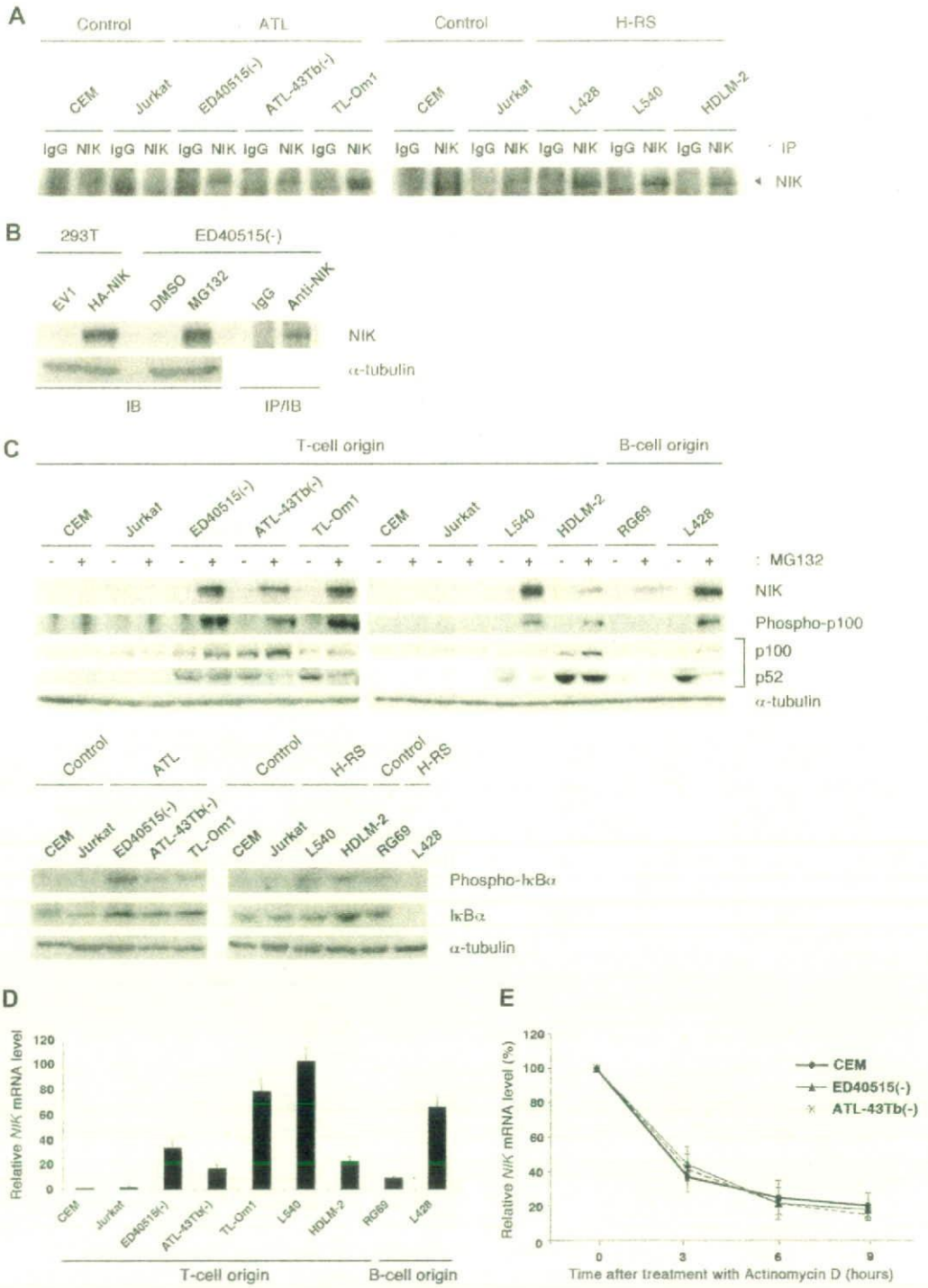

Figure 1. NIK protein is overexpressed in established ATL and Hodgkin Reed-Sternberg cells. (A) Steady-state levels of NIK expression in the ATL and H-RS cell lines were revealed by immunoprecipitation-coupled immunoblotting. Approximately 2×10^7 cells were lysed with buffer A. After preclearing, immunoprecipitation was performed at 4°C, using anti-NIK antibody (NIK) or its isotype IgG (IgG). After 3 washes with TNT buffer, immune complexes were analyzed by immunoblotting with anti-NIK antibody. (B) 293T cells were transfected with pMRX-HA-iresPuro or pMRX-HA-NIKiresPuro for 24 hours. Whole-cell lysates were used as negative and positive controls. ED40515(−) cells were pretreated with (+) or without (−) MG132 (20 μM) for 3 hours, lysed with RIPA buffer, and subjected to immunoblotting with anti-NIK or anti-α-tubulin antibodies. Immunoprecipitation-coupled immunoblotting was performed as in panel A. (C) Top panels: control T-cell lines (CEM and Jurkat), leukemic cell lines derived from ATL patients that do not express Tax (ED40515(−), ATL43-Tb(−), and TL-Om1, a control B-cell line (RG69), and H-RS cell lines (HDLM-2 and L540) were pretreated with (+) or without (−) MG132 (20 μM) for 3 hours, and 30 μg of the whole-cell extracts were subjected to Western blot analysis with the antibodies to the indicated proteins. Bottom panels: Whole-cell extracts from the indicated cell lines were analyzed by Western blotting with the antibodies to the indicated proteins. (D) Total RNA was extracted from the indicated cell lines and subjected to real-time RT-PCR to quantify the *NIK* mRNA levels. The *NIK* mRNA levels were normalized to *18S* RNA. The relative *NIK* mRNA levels shown represent the fold increases in mRNA abundance, relative to that of the CEM cells (arbitrarily set at 1). (E) Cells were cultured in the presence of actinomycin D (5 μg/mL) for the times indicated, and then total RNA was isolated and subjected to quantitative RT-PCR as in panel D. Data are expressed as mean plus or minus SD of 3 independent experiments. The relative amounts of *NIK* mRNA shown represent the percentages in mRNA abundance, relative to that of each cell line before the addition of actinomycin D (arbitrarily set at 100%). IB indicates immunoblotting; IP, immunoprecipitation.

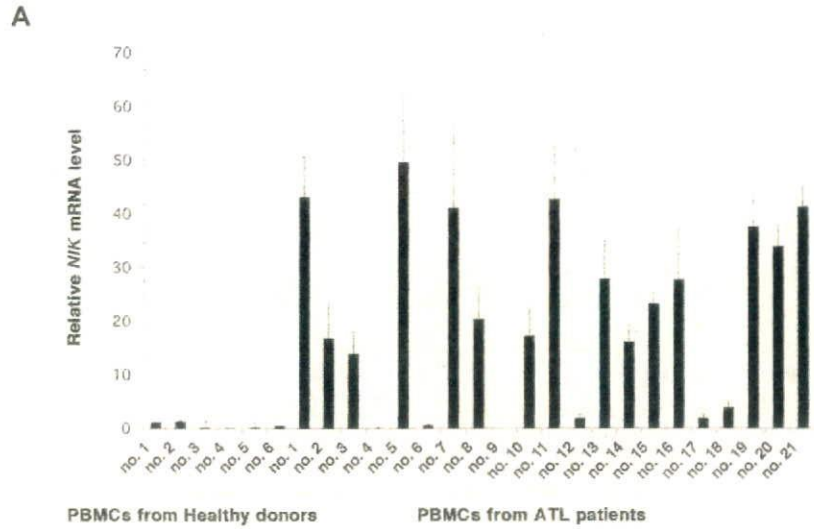

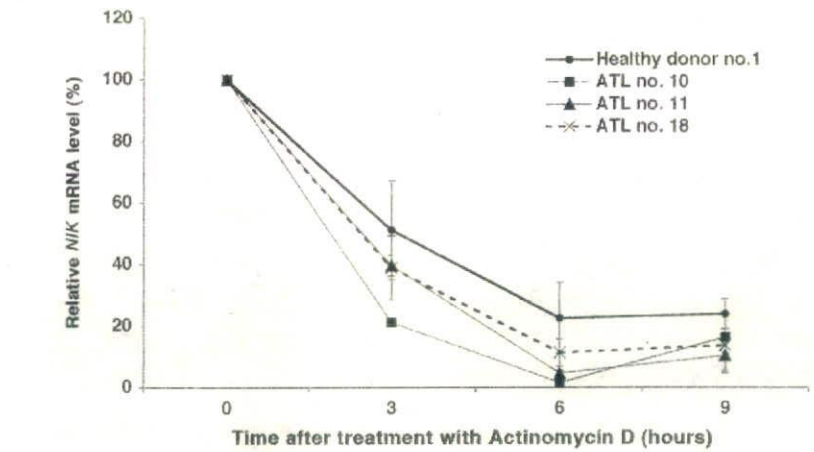

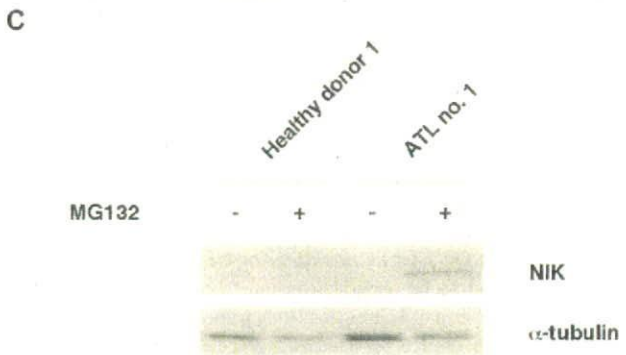

Figure 2. Overexpression of the *NIK* mRNA and protein in PBMCs from ATL patients. (A) Total RNA was extracted from PBMCs from healthy donors and ATL patients and then subjected to quantitative RT-PCR. The *NIK* mRNA levels were normalized to *18S* RNA. The relative *nik* mRNA levels shown represent the fold increases in mRNA abundance relative to that of healthy donor 1 (arbitrarily set at 1). These data are expressed as the mean plus or minus SD of 3 independent experiments. (B) PBMCs were cultured in the presence of actinomycin D (5 μg/mL) for the times indicated, and then total RNA was isolated and subjected to quantitative RT-PCR. The relative amounts of *NIK* mRNA shown represent the percentages in mRNA abundance, relative to that of PBMCs before the addition of actinomycin D (arbitrarily set at 100%). (C) PBMCs from a healthy donor and an ATL patient were treated with (+) or without (−) MG132 (20 μM) for 3 hours, lysed with RIPA buffer, and subjected to immunoblotting with anti-NIK or anti-α-tubulin antibodies.

expressed this protein (Figure 3A) without significant morphologic change (Figure 5B) or constitutive NF-κB activation (Figure 3C). As expected, these cells failed to survive selection with blasticidin S (data not shown).

The expression of wild-type NIK in B5 and h12 cells potently induces p52 expression and NF-κB DNA binding activity, whereas the catalytically inactive NIK mutant does not (Figure 3B,C). We also found a specifically phosphorylated form of IκBα in cells expressing wild-type NIK (Figure 3A). Super-shift experiments revealed that the NF-κB–DNA binding complexes in B5 and h12 cells expressing NIK involve p50, RelB, and RelA (Figure 4D). The presence of p52 in the DNA binding complexes could not be examined, however, because an antibody recognizing rat p52 in super-shift assay is not currently available. Instead, we analyzed DNA-binding complexes induced by NIK expression in wild-type mouse embryonic fibroblasts (Figure S2). Retroviral overexpression of NIK indeed induced DNA-binding NF-κB complexes containing p52, and enhanced expression of p52 and phosphorylated form of IκBα.

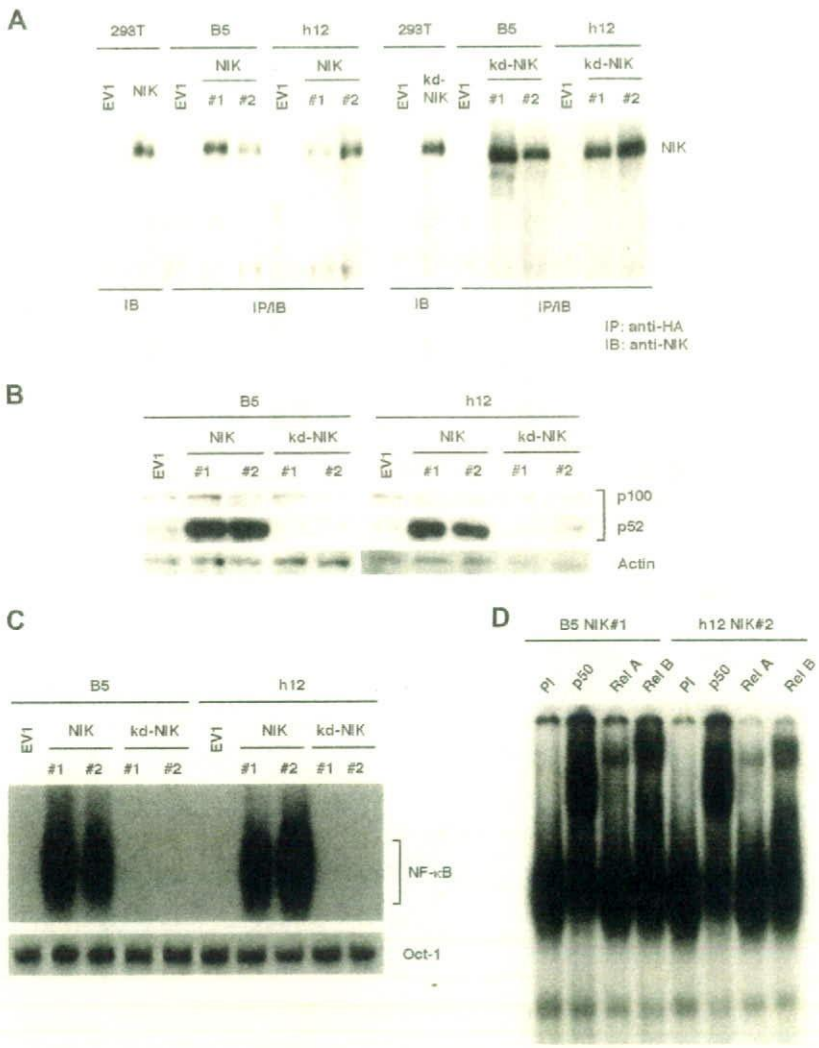

Figure 3. NIK induces constitutive NF-κB activity in rat fibroblasts. (A) B5 and h12 cells were infected with retroviruses capable of expressing HA-tagged NIK (NIK) or catalytically inactive NIK (kd-NIK). Pools of B5 and h12 cells transduced with the control pMRX-HAiresPuro vector (EV1) were used as a control. Cytoplasmic extracts from EV1 and 2 independent cell clones (no. 1 and no. 2) were subjected to immunoprecipitation using antibody against the HA epitope. Immunoprecipitates were then resolved by 8% SDS-PAGE and subjected to immunoblotting with anti-NIK antibody. 293T cells were transiently transfected with the pMRX-HAiresPuro vector (EV1) or pMRX-HA-NIKiresPuro (NIK). Cytoplasmic extracts (30 μg) were then used for immunoblotting as negative and positive controls, respectively. (B) Elevated p52 production in rat fibroblasts. Whole-cell lysates from B5 and h12 cells expressing wild-type NIK or kd-NIK were subjected to SDS-PAGE and immunoblotting with anti-p52 for detection of p100 and p52 or antiactin antibodies. (C) Elevated NF-κB–DNA binding activity in rat fibroblasts; 5 μg of nuclear extracts prepared from B5 and h12 cells expressing wild-type NIK or kd-NIK were analyzed by EMSA, using oligonucleotides encoding an NF-κB–binding sequence or Oct-1–binding sequence as probes. (D) DNA-binding NF-κB components in B5 and h12 cells expressing wild-type NIK were analyzed by super-shift EMSA. Nuclear extracts (5 μg) from B5 NIK#1 and h12 NIK#2 cells were preincubated for 30 minutes with preimmune (PI), anti-p50, anti-RelA or anti-RelB sera, and then subjected to EMSA with the NF-κB–specific probe. IB indicates immunoblotting; IP, immunoprecipitation.

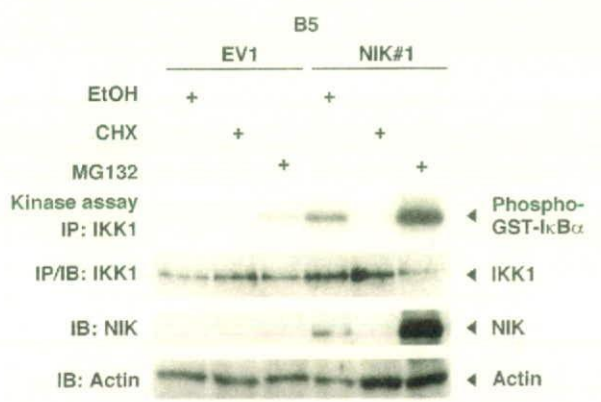

Figure 4. NIK expression parallels IKK activity after CHX or MG132 treatment. B5 cells transduced with the control vector (EV1) or B5 cells expressing wild-type NIK (NIK#1) were treated for 4 hours with either vehicle (ethanol, EtOH), cycloheximide (CHX; 50 μg/mL), or MG132 (20 μM). Cytoplasmic extracts were subjected to immunoprecipitation with IKK1-specific antibody, and then immunoprecipitates were used for an in vitro kinase assay. IKK1 expression in the immunoprecipitates was revealed by immunoblotting with IKK1-specific antibody. NIK and actin levels in the cytoplasmic extracts used for immunoprecipitation were determined by immunoblotting with anti-NIK or antiactin antibodies, respectively. IB indicates immunoblotting; IP, immunoprecipitation; GST, glutathione-S-transferase tag.

We have previously demonstrated that the treatment of ATL cells with MG132 greatly enhances IKK activity, whereas protein synthesis inhibition quickly abolished this activity.[11] Figure 4 shows that the IKK activity in B5 cells stably expressing NIK (NIK#1) is modulated by MG132 and cycloheximide (CHX) in a manner that is very similar to that seen in ATL cells. In addition, treatment of NIK#1 cells with MG132 remarkably elevates the level of exogenous NIK expression. The constitutive NF-κB activation caused by the presence of exogenous NIK was found to be abolished by the retroviral expression of a super-repressor form of IκBα (SR-IκBα), without affecting exogenous NIK expression (Figure 5A). Interestingly, the forced expression of SR-IκBα also diminishes the p52 and p100 expression levels.

We next tested the ability of NIK to induce anchorage-independent growth of rat fibroblasts. B5 and h12 cells transduced with the control vector did not form colonies of significant size in soft agar, whereas those transduced with wild-type NIK expression vector formed a number of large colonies, as shown in Figure 5B and Table 1. Cells expressing catalytically inactive NIK failed to form colonies in soft agar. The expression of SR-IκBα completely abolished NIK-induced colony formation and also the morphologic alterations of B5 and h12 cells. Given that SR-IκBα specifically suppresses NF-κB activation,

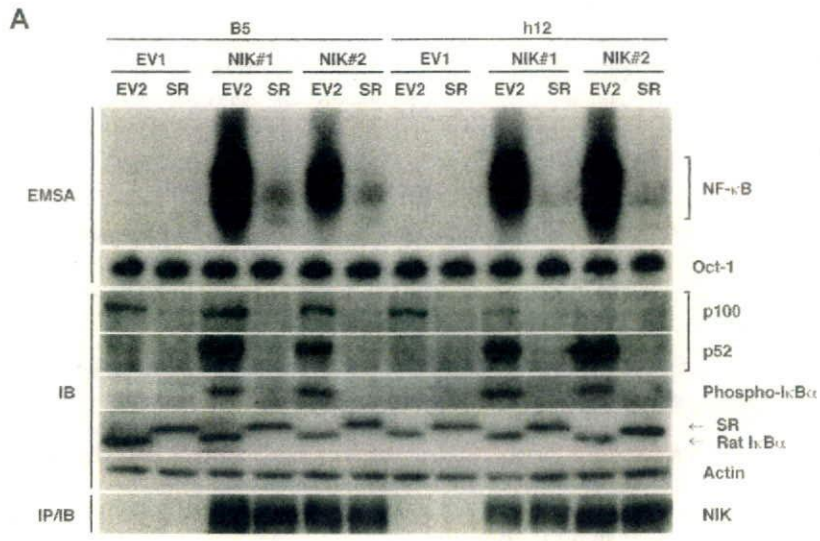

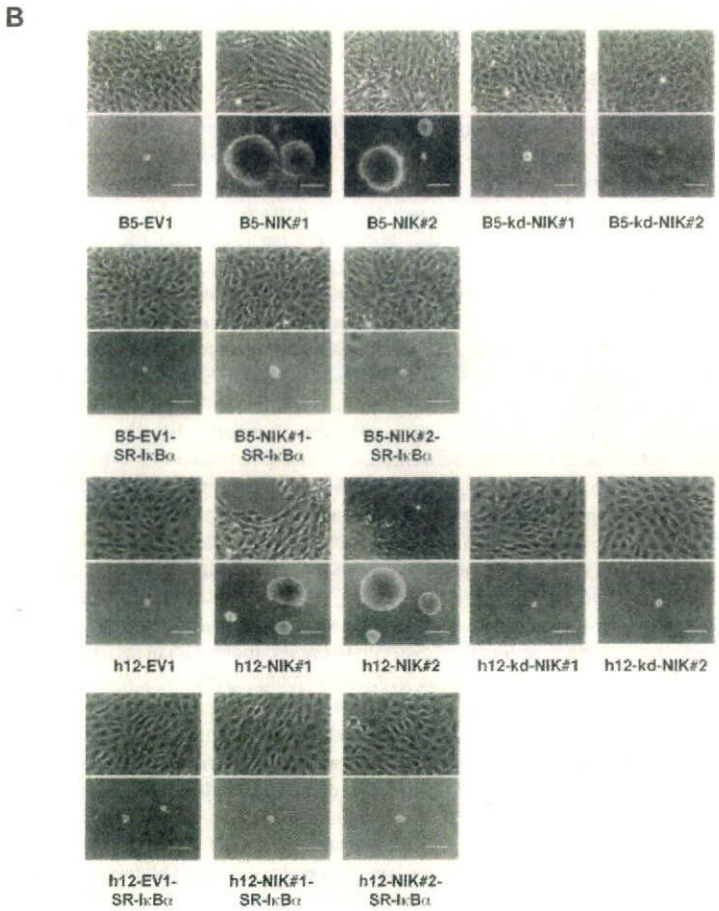

Figure 5. The overexpression of NIK transforms rat fibroblasts in an NF-κB–dependent manner. (A) Top 2 panels: 5 μg of nuclear extracts prepared from B5 and h12 cells transduced with empty vector (EV2) or SR-IκBα (SR) were analyzed by EMSA, using NF-κB and Oct-1 probes. Middle 5 panels: whole-cell extracts (30 μg) of B5 or h12 infectants were subjected to SDS-PAGE and immunoblotting with anti-p52, antiphospho-IκBα, anti-IκBα, or antiactin antibodies. Bottom panel: HA-tagged NIK was immunoprecipitated from B5 and h12 infectants with anti-HA antibody and detected by immunoblotting with anti-NIK antibody (H-248). (B) Phase-contrast micrographs of cells cultured on monolayers (top images) or in soft agar (bottom images). B5 or h12 cell clones expressing wild-type NIK (NIK#1 and NIK#2) or not (EV1) were cultured in soft agar for 3 weeks. These cells were further transduced with SR-IκBα, and then pooled cells were assayed for anchorage-independent growth in soft agar. B5 and h12 cell clones expressing kd-NIK were also examined. Original magnification ×100. Scale bar represents 100 μm. SR indicates super-repressor; kd-NIK, catalytically inactive NIK; IB, immunoblotting; IP, immunoprecipitation.

we conclude from these results that NIK transforms rat fibroblasts in an NF-κB–dependent manner.

NIK mediates constitutive NF-κB activation in ATL cells

The similar modulation of IKK activity by CHX or MG132 in both ATL and B5 cells expressing NIK (Figure 4) suggests that NIK plays an important role in constitutive NF-κB activation in ATL cells. We therefore examined whether the RNA interference-mediated silencing of endogenous *NIK* gene expression would lower NF-κB–dependent transcription in these cells. ED-40515(−) and ATL-43Tb(−) cells were infected with lentiviral constructs that express short hairpin RNA (shRNA) molecules that target mRNA for either *Renilla luciferase* (Ctli) or *NIK* (NIKi), and then subjected to puromycin selection for 2 days. To